






Article

Green Synthesis of Gold Nanoparticles by Aqueous Extract of *Zingiber officinale*: Characterization and Insight into Antimicrobial, Antioxidant, and In Vitro Cytotoxic Activities

Amr Fouda ^{1,*}, Ahmed M. Eid ¹, Eric Guibal ^{2,*}, Mohammed F. Hamza ^{3,4}, Saad El-Din Hassan ¹, Dalal Hussien M. Alkhalifah ⁵ and Dalia El-Hossary ⁶

¹ Botany and Microbiology Department, Faculty of Science, Al-Azhar University, Nasr City, Cairo 11884, Egypt

² Polymers Composites and Hybrids (PCH), IMT Mines Ales, F-30319 Alès, France

³ School of Nuclear Science and Technology, University of South China, Hengyang 421001, China

⁴ Nuclear Materials Authority, P.O. Box 530, El-Maadi, Cairo 11728, Egypt

⁵ Department of Biology, College of Science, Princess Nourah Bint Abdulrahman University, P.O. Box 84428, Riyadh 11671, Saudi Arabia

⁶ Department of Medical Microbiology and Immunology, Faculty of Medicine, Zagazig University, Zagazig 44519, Egypt

* Correspondence: amr_fh83@azhar.edu.eg (A.F.); eric.guibal@mines-ales.fr (E.G.);

Tel.: +20-1113351244 (A.F.); +33-(0)-4667-82734 (E.G.)

Abstract: The main challenge for researchers in the biomedical sectors concerns the development of new active compounds through cost-effectiveness, rapid, simple, and ecofriendly methods to overcome antibiotic resistance to pathogenic microbes. Herein, gold nanoparticles (AuNPs) were fabricated by a green approach through the reduction of chloroauric acid (HAuCl₄) by harnessing the metabolites present in the aqueous extract of *Zingiber officinale* rhizome. UV-Vis spectroscopy, FT-IR, XRD, TEM, DLS, and zeta potential were used to characterize phytosynthesized AuNPs. In addition, the antimicrobial effect was investigated against Gram-positive bacteria (*Bacillus subtilis* and *Staphylococcus aureus*), Gram-negative bacteria (*Pseudomonas aeruginosa* and *Escherichia coli*), unicellular fungi (*Candida albicans*), and multicellular fungi (*Aspergillus brasiliensis*). Antioxidant and in vitro cytotoxic activities were assessed. TEM and XRD showed the successful formation of spherical and crystalline structures, with sizes in the range of 5–53 nm (average size: 15.11 ± 8.5 nm). The zeta potential value (i.e., −28.8 mV) explains the high stability of synthesized AuNPs. AuNPs exhibit promising activity against prokaryotic and eukaryotic microorganisms with variable inhibition zones and low MIC values in the range of 25–6.25 µg mL^{−1}. Phytosynthesized AuNPs exhibit DPPH scavenging activity with percentages of 87.6 ± 0.5% at a maximum concentration (1000 µg mL^{−1}), which can be compared with ascorbic acid (97.3 ± 0.2%). Moreover, the AuNPs displayed a target-oriented effect for cancer cell lines HepG2 and MCF7 at low IC₅₀ concentrations of 131.9 ± 9.34 and 288.23 ± 31.39 µg mL^{−1} compared to the normal oral epithelial OEC cell line (487.612 ± 3.53 µg mL^{−1}). Overall, the phytosynthesized AuNPs show wide activities that enable their use in various biomedical and biotechnological applications.

Keywords: green synthesis; ginger rhizome extract; gold nanoparticles; DPPH; pathogenic microbes; normal and cancerous cell lines



Citation: Fouda, A.; Eid, A.M.; Guibal, E.; Hamza, M.F.; Hassan, S.E.-D.; Alkhalifah, D.H.M.; El-Hossary, D. Green Synthesis of Gold Nanoparticles by Aqueous Extract of *Zingiber officinale*: Characterization and Insight into Antimicrobial, Antioxidant, and In Vitro Cytotoxic Activities. *Appl. Sci.* **2022**, *12*, 12879. <https://doi.org/10.3390/app122412879>

Received: 10 November 2022

Accepted: 13 December 2022

Published: 15 December 2022

Publisher's Note: MDPI stays neutral with regard to jurisdictional claims in published maps and institutional affiliations.



Copyright: © 2022 by the authors. Licensee MDPI, Basel, Switzerland. This article is an open access article distributed under the terms and conditions of the Creative Commons Attribution (CC BY) license (<https://creativecommons.org/licenses/by/4.0/>).

1. Introduction

Diseases caused by various pathogenic bacteria and fungi are considered the main source of morbidity and mortality worldwide. Moreover, the inappropriate use of antibiotics has caused the emergence of new strains that are resistant to most antibiotics (antimicrobial resistance, AMR) [1]. The WHO has also declared cancer (uncontrolled cell division) as one of the leading causes of death in the world. Chemotherapy has emerged as one of the most widely used treatments for various types of cancer, but relevant protocols

involve a combination of cytotoxic agents such as alkylating agents and anti-metabolic agents. Unfortunately, improper application of chemotherapy leads to the development of multidrug resistance and causes patients to suffer severe side effects. This requires the development of new treatments. Biologically active ingredients such as plant extracts and natural dietary ingredients associated with nanomaterials have been revealed as promising alternatives [2,3]. Nanoparticles (NPs) are the basic building block of nanotechnology and have at least one dimension in the nanometric scale range of 1–100 nm. These materials have unique chemical, physical, and mechanical properties that justify their application in many fields, such as agriculture, wastewater treatment, textile industry, energy, catalysis, adsorption of heavy metals, medicine, and cosmetics [4,5]. For instance, silver nanoparticles (AgNPs) fabricated by root extract of *Helicteres isora* exhibit antibacterial and antioxidant activities [6]. High antibacterial activity was obtained against Gram-negative bacteria (*Salmonella typhi* and *Pseudomonas aeruginosa*) compared with Gram-positive bacteria (*Bacillus subtilis* and *Micrococcus luteus*). Moreover, synthesized AgNPs showed promising antioxidant activity, which was characterized by the DPPH method, a reducing power assay, and scavenging of nitric oxide radicals and hydrogen peroxide. In a recent study, selenium nanoparticles (SeNPs) synthesized by harnessing an aqueous extract of *Portulaca oleracea* showed antimicrobial, antiviral cytotoxicity in vitro, as well as mosquitocidal activities [7].

Nanomaterials and nanocolloids can be manufactured by physical, chemical, and biological methods [8]. The biofabrication of nanomaterials using extracts of plants and microorganisms is very interesting for avoiding pressures, high temperatures, and hazardous chemicals. The high stability of green synthesized nanomaterials is associated with the capping effect of the plant extract [9–11]. Moreover, the technique is environmentally friendly and biologically safe, as well as being low-cost [12,13]. Among the various biological methods for the production of nanoparticles, plants are very attractive for green synthesis due to their diversity and ease of use. In addition, plant extracts contain a large number of phytochemicals that may combine different roles, such as reducing and/or stabilizing agents for the production of nanomaterials [14–17]. Biogenic NPs have been adapted and applied in many important fields of biotechnology, such as tissue engineering, health and medicine, drug delivery, pharmacology, cosmetics, nanodiagnostics, and agriculture [18,19]. Recently, gold NPs have become a topic of interest due to their volumetric and morphological properties that can be modulated by their electrical, optical, physical, and chemical characteristics. These particles have been used in many technological applications, such as optoelectronics, nanoelectronics, and biological and chemical sensors, in addition to their biomedical applications in controlled drug delivery and release and bioimaging [20]. Moreover, gold NPs exhibit outstanding sensitivity and selectivity for the colorimetric identification of toxic heavy metal ions [21]. In this context, nanogram doses of gold NPs manifested potential activity against multidrug-resistant pathogens, as well as against *Candida albicans*; therefore, they were employed as a coating for medical devices [22]. Owing to their low toxicity, AuNPs were used in oral biology and for the coating of urological catheters [22]. AuNPs may reduce nosocomial infections [23]. Furthermore, the cytopathic effect of the herpes simplex virus was considerably reduced in vitro by nontoxic concentrations of AuNPs [24]. On the other hand, the phytofabricated AuNPs displayed premium free radical scavenging performance [25]. Plant extracts have been widely used to produce AuNPs; for example, *Aloe vera*, *Azadirachta indica*, *Cinnamomum camphora*, *Medicago sativa*, *Terminalia catappa*, and *Coriandrum sativum* have been reported as highly efficient agents for the synthesis of AuNPs [26]. It is noteworthy that AuNPs are generally considered less cytotoxic than alternative metal NPs [27,28]. This was another motivation for investigating plant-extract-mediated synthesis of AuNPs.

Ginger (*Zingiber officinale*; Zingiberaceae) is a herbaceous, perennial plant that has been used for centuries as a condiment for food and beverages, as well as in folk medicine for recovery from cough and flu and gastrointestinal diseases, as well as its anti-inflammatory, antinausea, and digestion-aiding activity, in addition to promoting the body's immunity

level [29]. Ginger contains many active metabolites, including volatile oils, as well as non-volatile compounds, such as paradols, zingerone, shogaols, and gingerols, which are believed to be responsible for the distinctive biological and medicinal characteristics of ginger [30]. Scientific reports have proven the pharmacological effects of ginger as antibacterial, anticancer, antioxidant, antidiabetic, analgesic, and anti-inflammatory activities [29,31,32]. In addition to helping treat and prevent arthritis, it has hepatoprotective and nephroprotective effects [33–35]. The propensity of ginger extract to facilitate the synthesis of metal nanoparticles was previously reported for copper [36], silver [37], and gold [38].

The current study investigates the biogenic synthesis of AuNPs by using aqueous extract of fresh ginger rhizome for the reduction of HAuCl₄. After evaluating the physico-chemical characteristics of the phytosynthesized nanoparticles, we explore their potential biological activity in terms of antioxidant, antimicrobial, and cytotoxic effects. The objective of this study is to evaluate the possible fields of application of AuNPs and their limitation for practical uses.

2. Materials and Methods

2.1. Materials

Chloroauric acid (HAuCl₄, 99%) was used as a metal precursor and obtained from Sigma Aldrich (Darmstadt, Germany). Nutrient agar media comprised peptone, 5; beef extract, 3; NaCl, 5; and Agar, 15 g L⁻¹. Yeast extract peptone dextrose (YEPD) agar was prepared with peptone, 20; yeast extract, 10; dextrose, 20; and agar, 15 g L⁻¹. Czapek Dox agar contained sucrose, 30; NaNO₃, 2; K₂HPO₄, 1; MgSO₄, 0.5; KCl, 0.5; FeSO₄, 0.01; and agar, 15 g L⁻¹. All media components were purchased from Sigma Aldrich (Cairo, Egypt). The strains of pathogenic organisms were obtained from Microbial Physiological Lab., Faculty of Science, Al-Azhar University. Antimicrobial activity was achieved using Muller–Hinton agar media (Read-prepared, Sigma Aldrich, Merck, Germany). Moreover, cancer and normal cell lines used in the current study were purchased from the Holding Company for Biological Products and Vaccines (VACSERA), Cairo, Egypt.

2.2. *Zingiber Officinale*-Mediated Green Synthesis of AuNPs

The rhizome of *Z. officinale* was purchased from a local Egyptian supermarket and washed thrice with tap water to remove any adhering particles. Rhizome (10 g) was cut into small parts and mixed with 100 mL distilled H₂O under stirring conditions (100 rpm) at 60 °C for 60 min before being centrifugated at 1000 rpm for 10 min; the supernatant was used for green synthesis of AuNPs.

For green synthesis, 1 mL of stock solution of HAuCl₄ (100 mM) was added to 100 mL of collected supernatant (to obtain a final concentration of 1 mM). The mixture was stirred at 60 °C for 60 min; the pH of the mixture was adjusted to 8 using 1 M NaOH solution at the beginning of the stirring step. A color change from pale yellow (plant aqueous extract) to purple indicated the successful formation of AuNPs [39]. The solution was evaporated to collect the precipitate, which was washed thrice with sterilized distilled H₂O followed by oven drying at 200 °C for one hour. The different steps for green synthesis of AuNPs using the aqueous extract of *Z. officinale* rhizome are represented in Figure 1.

2.3. Characterization

The first indication for successful green synthesis of AuNPs using plant aqueous extract is provided by the color change of the solution. The purple color intensity was monitored by measuring the absorbance of the solution at a wavelength varying between 200 and 800 nm using UV-visible spectroscopy (JENWAY 6305 spectrophotometer, Jenway, Bibby Scientific UK, Staffordshire, UK). In this assay, 2 mL of synthesized purple solution was added to a quartz cuvette, and the spectrum was monitored at regular intervals of time to detect the maximum surface plasmon resonance (SPR) [40].

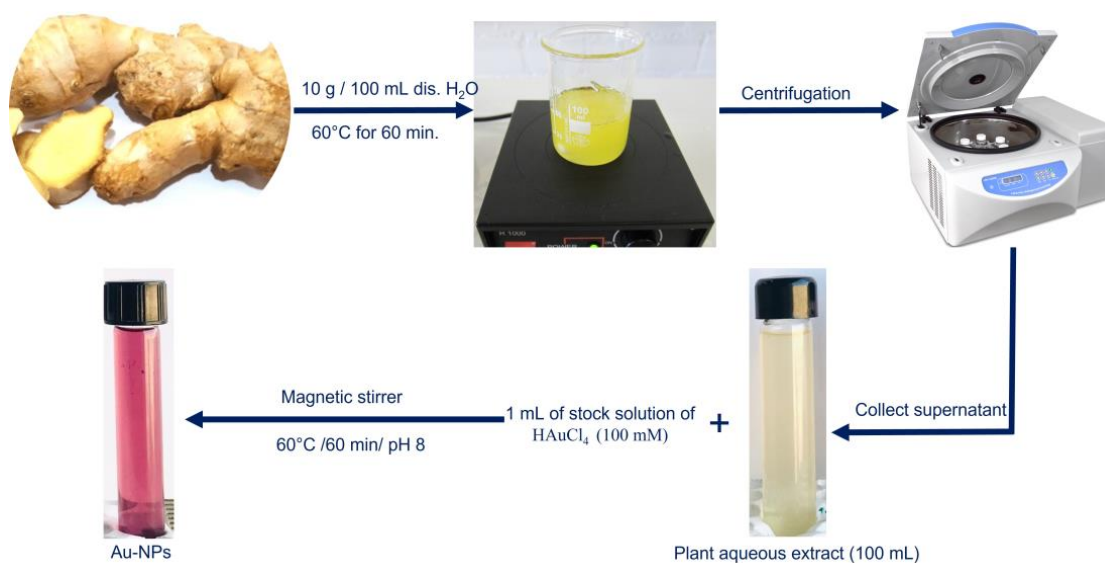


Figure 1. Scheme for green synthesis of AuNPs using the aqueous extract of *Z. officinale* rhizome.

The various functional groups related to specific molecules or metabolites in plant aqueous extract and their role in the reduction and stabilization of as-formed AuNPs were assessed using Fourier transform infrared (FT-IR) [41]. In this method, 10 mg of synthesized AuNP powder or 3 mL of plant aqueous extract was well-mixed with KBr, left to completely dry, and compressed to form a loaded KBr disk. The spectra were acquired by scanning in the range of 400–4000 cm^{-1} using FT-IR spectrophotometry (JASCO FT-IR 4100 spectrometer, Jasco Co., Hachioji, Tokyo, Japan).

The morphological characteristics (shape and size) of plant-based AuNPs were investigated by transmission electron microscopy (TEM) (JEOL JEM-1010, JEOL, Tokyo, Japan). The synthesized AuNPs were suspended in ultrapure water (Milli-Q water) and submitted to sonification to ensure effective dispersion. A few drops of the suspended solution were loaded on the TEM carbon grid and left to dry before being analyzed by TEM.

The crystalline nature of as-formed AuNPs was characterized by X-ray diffraction analysis using a PANanalytical-X'Pert-Pro-MRD apparatus (Almelo, the Netherlands) equipped with a Cu K_{α} source ($\lambda = 1.5406 \text{ \AA}$). Operating conditions were set at 40 kV voltage and 30 mA current. Scanning was performed in the range of 2θ values of 5–80°. The average value of crystallite size for synthesized AuNPs was calculated using the Debye–Scherrer equation applied to the experimental XRD pattern [42]:

$$\text{Average crystallite size} = \frac{K \times \lambda}{\beta \times \cos \theta} \quad (1)$$

where K is the Scherrer constant (i.e., 0.94), β is the full width of the diffraction peak at a half maximum, and θ is the diffraction angle.

The size distribution in the colloidal solution was assessed by dynamic light scattering (DLS, Nano-ZS, Malvern Ltd., Malvern, UK). The synthesized AuNPs were dispersed under ultrasonification in high-purity water (Milli-Q H_2O) to avoid extra peaks or appearance of shadows on peaks during the scattering. The measurement was performed in triplicate at $T: 24.6 \text{ }^{\circ}\text{C}$, $\text{pH} \approx 6.5$; the refractive index was 1.33, and the loading index was 2.56. Finally, the surface charge of AuNPs was investigated by a zetasizer (Nano-ZS, Malvern, UK) using the Smoluchowski model. Electrokinetic measurements were performed at $T: 25 \text{ }^{\circ}\text{C}$, $\text{pH} \approx 6.5$ in highly pure water. Twelve zeta runs were operated, and the count rate was 55.2 kcps.

2.4. Antimicrobial Activity

An agar well diffusion assay was employed to explore the antimicrobial properties of plant-based AuNPs against a group of potentially pathogenic samples including

Escherichia coli ATCC8739 and *Pseudomonas aeruginosa* ATCC9027 as Gram-negative bacteria, *Bacillus subtilis* ATCC6633 and *Staphylococcus aureus* ATCC6538 as Gram-positive bacteria, *Candida albicans* ATCC10231 as unicellular fungi, and *Aspergillus brasiliensis* ATCC16404 as multicellular fungi [43]. The nutrient agar, YEPD agar, and Czapek Dox agar media were used to subculture the bacterial strains and unicellular and multicellular fungi, respectively. Microorganisms were incubated at 35 ± 2 °C for 24 h for bacteria and *C. albicans* and at 25 ± 2 °C for 72 h for *A. brasiliensis*. After overnight growth, single colonies from separate bacterial strains and unicellular fungi were picked up using a sterile swab and spread uniformly on a Muller–Hinton agar plate (Ready-prepared, Oxoid Ltd., Altrincham, UK), whereas approximately 50 µL of spore suspension of *A. brasiliensis* was spread over the surface of Czapek Dox agar media. Then, four wells (0.7 mm in diameter) were prepared in each plate before being filled with 100 µL of AuNP solutions (200, 100, 50, 25, 12.5, 6.25, and 3.12 µg mL⁻¹). The DMSO (solvent system) was systematically used as a control. The loaded plates were incubated at 35 ± 2 °C for 24 h for bacteria and *C. albicans* and at 25 ± 2 °C for 72 h for *A. brasiliensis*. The results were recorded as the diameter of clear zones (mm) formed around each well after the selected incubation period. The minimum inhibitory concentration (MIC) for each organism was detected as the lowest concentration of synthesized AuNPs that formed a clear zone. The experiments were performed in triplicate, and the data are represented as average values and standard deviation intervals.

2.5. Antioxidant Activity Using DPPH Free Radical Scavenging Assay

The antioxidant potential of *Z. officinale*-derived AuNPs was evaluated by a DPPH (2,2-diphenyl-1-picrylhydrazyl) free radical scavenging assay. Double-fold concentrations of AuNPs with ascorbic acid as a standard (1000–1.95 µg mL⁻¹) were prepared in Milli-Q water. One mL of each concentration of the gold colloidal solution and ascorbic acid was dispensed in a test tube. Then, 1 mL of 0.1 M DPPH (dissolved in methanol) and 450 µL of Tris-HCl buffer (50 mM/pH 7.4) were added before incubating under shaker conditions (100 rpm) at 37 °C for 30 min in the dark. Another set of experiments was achieved by replacing AuNPs or ascorbic acid with one mL of Milli-Q and running as a blank. The absorbance of the formed color was measured at 517 nm [44]. The percentage of radical-scavenging efficiency was calculated by the following equation:

$$\text{Scavenging inhibition (\%)} = \frac{\text{Absorbance of control} - \text{Absorbance of test sample}}{\text{Absorbance of control}} \times 100 \quad (2)$$

2.6. In Vitro Cytotoxic Assay

The in vitro cytotoxicity of the ginger-fabricated AuNPs was evaluated against HepG2 (hepatocellular carcinoma), MCF7 (adenocarcinoma), and OEC (normal oral epithelial) cell lines by MTT (3-(4,5-dimethylthiazol-2-yl)-2,5-diphenyl tetrazolium bromide) assay method. Each cell line was seeded in 96-well tissue culture plates (1×10^5 cells/100 µL/well) and incubated under a 5% CO₂ atmosphere for 24 h at 37 °C. Then, the monolayer cell sheet was washed twice by washing media before adding the maintenance media (RPMI medium with 2% serum). Thereafter, cells were treated with various concentrations of the biogenic AuNPs (31.25, 62.5, 125, 250, 500, and 1000 µg mL⁻¹) and incubated for 48 h, with three wells free of NPs used as controls. After completion of the incubation, the media were poured from the plates; each well received 50 µL of fresh MTT solution in phosphate-buffered saline solution (PBS, 5 mg mL⁻¹) and was mixed thoroughly for 5 min; then, plates enveloped with aluminum foil were further incubated for 4 h at 37 °C. MTT solutions were dumped off, and 100 µL of DMSO (10%) was added to solubilize the formed formazan crystals. Plates were kept in dark and shaken for 30 min. Ultimately, absorbance was measured at 570 nm using an ELISA reader [45]. Cellular morphological changes were disclosed by inverted microscopy (ECLIPSE Ts2, Nikon, Shinjuku, Tokyo, Japan), whereas the percentages of cell viability were calculated by the following equation:

$$\text{Cell viability (\%)} = \frac{\text{Absorbance of treated sample}}{\text{Absorbance of control}} \times 100 \quad (3)$$

The IC₅₀ values were calculated using curve fitting (cubic spline) with Prism software (GraphPad Software, San Diego, CA, USA) by an algorithm described by Chambers et al. [46].

Results were statistically analyzed using SPSS v18 (SPSS Inc., Chicago, IL, USA). An analysis of variance (ANOVA) test was used for multiple sample comparison, followed by Tukey's multiple comparison test.

3. Results and Discussion

3.1. Green Synthesis of AuNPs

The green synthesis of nanoparticles for biomedical applications has received considerable attention due to the less harmful side effects of these compounds compared with those synthesized by chemical and physical methods [47]. The metabolites secreted by various biological entities, such as plants and microorganisms (i.e., bacteria, actinomycetes, fungi, yeast, and algae), are used as reducing and stabilizing agents to produce highly stable NPs. Plant extracts are preferred over other biological sources owing to their high metabolite production, avoiding the pathogenicity of microbes; direct one-step processing; and cost-effectiveness [7,48]. Herein, the aqueous extract of *Z. officinale* rhizome was used for the green synthesis of AuNPs. As reported previously, *Z. officinale* rhizome provides an enriched source for various constituents, such as terpenes, lipids, phenolic compounds, polysaccharides, organic acids, and volatile oils [49,50]. These metabolites were used as biocatalyst to reduce metals and their oxide to produce nanoscale structures, followed by capping and stabilization (mediated by the extracted compounds). Therefore, we anticipated the high potentiality of the aqueous extract of *Z. officinale* rhizome to form highly stable gold nanoparticles. In the current study, the appearance of purple color (upon direct addition of metal precursor to plant aqueous extract) indicated the successful formation of AuNPs. A purple color, which indicates the synthesis of AuNPs, was documented by Elia et al. [51] after mixing the aqueous extracts of *Lippia citriodora*, *Punica granatum*, *Salvia officinalis*, and *Pelargonium graveolens* with HAuCl₄ solution. Environmental factors (especially pH) are crucial parameters affecting both the synthesis and the aggregation of synthesized nanoparticles. Ramzan et al. [37] showed that alkaline conditions were necessary for the efficient synthesis of silver nanoparticles with wild ginger extract. They also demonstrated that the formation of AgNPs strongly depends on the molarity of silver and the type of ginger extract (aqueous extracts are more efficient than organic extracts, especially at low metal concentrations). The pH value is of critical importance in the biosynthesis of NPs. In the current study, pH values varying between 5 and 8 were applied during AuNP synthesis. A pH value close to 8 was selected as the most appropriate value to form a high-intensity purple color using the aqueous extract of *Z. officinale*. This phenomenon can be attributed to the activity of plant metabolites under alkaline conditions [52], contributing to an enhancement in the stability of AuNPs and preventing agglomeration or aggregation with aging [53].

3.2. Characterization of AuNPs

3.2.1. Morphological Observation—TEM

The shape, size, and aggregation of *Z. officinale*-mediated green synthesis of AuNPs was investigated by TEM. The active metabolites from ginger aqueous extract have the potential to form spherical nanoparticles, with well-dispersed nano-sized objects in the range of 5–53 nm (average size: 15.11 ± 8.5 nm, Figure 2A,B). This is of the same order of magnitude as the gold nanoparticles synthesized by the mycelium of *Mucor plumbeus* (i.e., 13–25 nm; average size: 17 ± 4 nm, [54]). Consistent with this study, Huang et al. [55] reported that the size of AuNPs fabricated by leaf aqueous extract of *Dillenia indica* was between 5 and 50 nm, whereas the average particle sizes of AuNPs synthesized by aqueous extract of *Garcinia mangostana* peel and *Mentha longifolia* leaf were 32.9 ± 5.3 nm and

36.4 nm, respectively [39,56]. The variation in average particle sizes could be attributed to metabolites that varied between the plants used as reducing, capping, and stabilizing agents. Taha [57] compiled the characteristics of a series of AuNPs prepared by plant-extract-mediated synthesis. Most of the NPs were spherical, with a large variety in size (from 10 to 120 nm) depending on the plant; some examples of cubic, hexagonal, or triangular structures have also been reported. The biological activities of synthesized nanomaterials depend on various factors, such as size, aggregation, shape, surface area, and surface charge [58]. For instance, glucose oxidation by gold nanoparticles was shape-dependent; cubic and spherical shapes were most active, followed by rods and polyhedrons [59]. The activity of nanomaterials is usually size-dependent; (a) smaller particles are more active than large ones, and (b) a large surface area is more favorable for biological and chemical reactivity. For instance, selenium nanoparticles fabricated by an aqueous extract of garlic displayed higher antimicrobial activity at a size of 21–40 nm than larger sizes (in the range of 41–50 nm) [60]. Therefore, the detection of size, shape, surface charge, and aggregation of synthesized NPs is a crucial step to understand their activity.

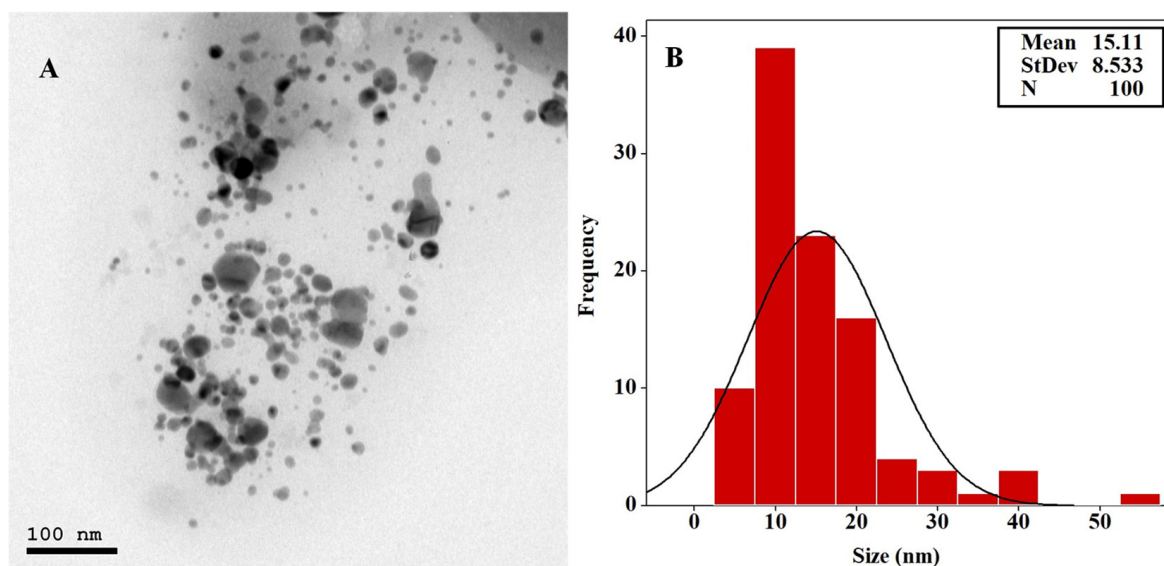


Figure 2. Transmission electron microscopy of AuNPs synthesized by aqueous extract of *Z. officinale* rhizome. (A) TEM image (spherical and well-dispersed NPs); (B): size distribution (determination based on TEM image analysis).

3.2.2. Crystallinity Characterization

The crystalline structure of phytosynthesized AuNPs was investigated by X-ray diffraction (XRD). As seen in Figure 3A, the XRD pattern shows four intense reflection peaks at 2θ degrees in the range of 5–80°. These peaks are identified at 2θ values of 38.2°, 44.4°, 64.7°, and 77.7°, which correspond to standard Bragg diffractions of the (111), (200), (220), and (311) planes, respectively. These diffraction peaks correspond to the face-center crystal lattice [40]. The obtained data are compatible with those reported for the green synthesis of AuNPs using plant extracts [56,61,62]. The obtained XRD pattern also confirms the crystalline nature of AuNPs according to the standard file of JCPDS No. 04-0784 [26]. The absence of extra diffraction peaks indicates the high purity of plant-based AuNPs. The average crystallite size of AuNPs was calculated according to the XRD pattern using the Debye–Scherrer equation [42]. The calculated size (i.e., 18 nm) is consistent with TEM analysis and with values reported for other plant-mediated AuNPs (i.e., approximately 12 nm for *Alternaria chlamyospora*-mediated gold nanoparticles [63] and 18 nm for *Coleus aromaticus* leaf extract [64]).

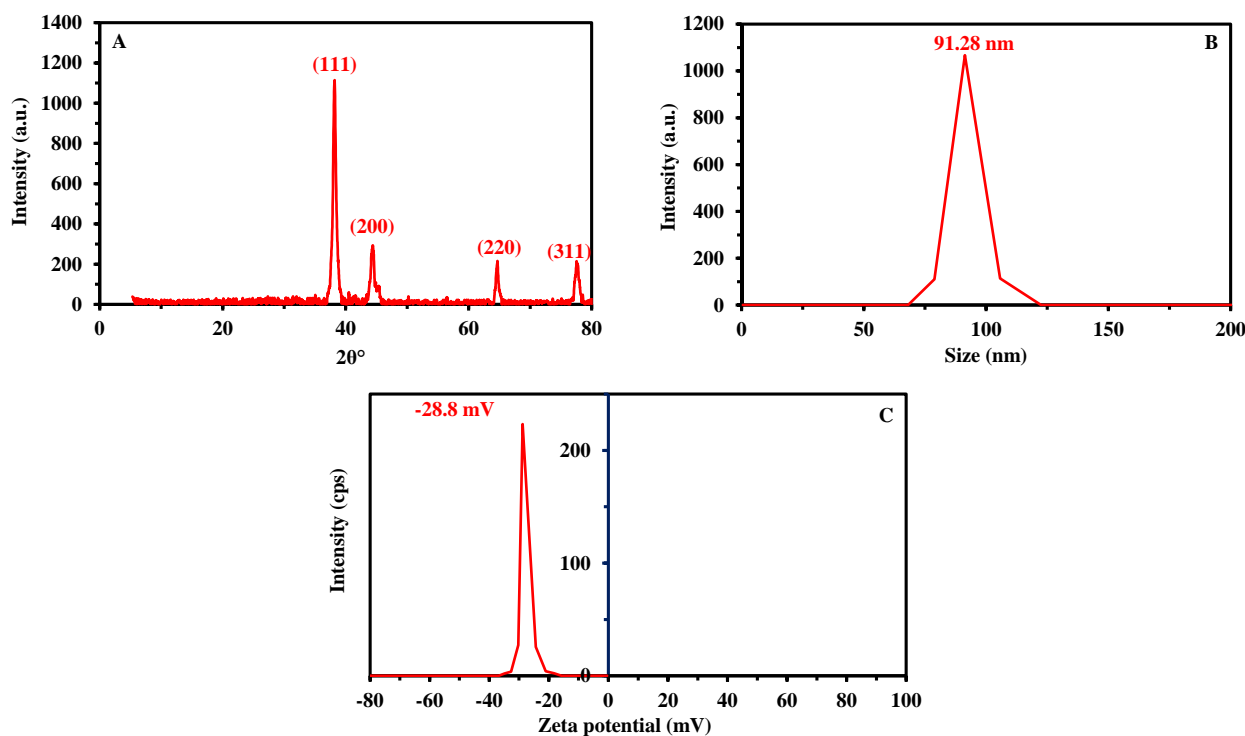


Figure 3. Characterization of AuNPs. (A) XRD analysis; (B) DLS measurements; (C) zeta potential analysis.

3.2.3. Particle Size Analysis—DLS

The size distribution and hydrodynamic residue of plant-based AuNPs can be detected by DLS analysis (diffraction light scattering). As shown in Figure 3B, the average size obtained from DLS analysis is about 91.28 nm according to the size distribution graph. Accordingly, the particle size obtained by DLS is larger than the values obtained by TEM and XRD (Table 1). This phenomenon could be explained by the fact that TEM analysis is performed on dry particles, as opposed to DLS (carried out in an aqueous solution), which measures the diameter in the hydrated state (hydrodynamic diameter) [65]. In addition, the diameter obtained by DLS is affected by the non-homogeneous distribution of NPs in the colloidal solution and the coating agent around the NPs surface, which may interfere with size calculation [66,67]. The average size of gold nanoparticles fabricated by aqueous extract of *Benincasa hispida* was close to 70 nm when measured by DLS analysis, whereas a much smaller size was obtained by TEM analysis (i.e., 22.2 nm) [41]. The average particle size of gold nanorods synthesized by biomass filtrate of *Nostoc ellipsosporum* was 436.6 nm and 173 nm when obtained by DLS and TEM analyses, respectively [53]. Despite the “increase” in relative particle size of AuNPs in their hydrated state, the particles maintained their nanometric order.

Table 1. The average size of green synthesized AuNPs calculated by TEM, XRD, and DLS.

| Size Measurement By: | Average Size |
|----------------------|----------------|
| TEM | 15.11 ± 8.5 nm |
| XRD | 18 nm |
| DLS | 91.28 nm |

Moreover, the polydispersity index (PDI) can be calculated using DLS data. A suspension can be considered homogeneous when the PDI (ranging between 0 and 1) remains below 0.4; on the other hand, when PDI exceeds 1, the distribution is fully heterogeneous [68]. Herein, the PDI value of green synthesized AuNPs in the colloidal solution was 0.3, meaning that dispersion was homogeneous.

3.2.4. Electrokinetic Potential—pH_{PZC}

The zeta or electrokinetic potential is the potential to move particles in a colloidal solution under an electric field [69]. It is a reproducible and easy-to-use tool for the detection of the stability of biosynthesized NPs. As shown, the zeta value of synthesized AuNPs was -28.8 mV, which confirms the stability of nanoparticles (Figure 3C). For AuNPs synthesized in the presence of Red Dragon pulp and seed oil, Al-Radadi [40] reported zeta potential values close to -18.4 mV. The guideline for classifying the stability of NPs based on zeta potential analysis was reported as follows: ± 0 – 10 mV corresponds to highly unstable particles and ± 10 – 20 mV is defined as relatively stable, whereas ± 20 – 30 mV and $> \pm 30$ mV are moderate and highly stable, respectively [70]. The results show that plant-based AuNPs have a relatively high negative surface charge and stability. This stability should be also investigated in the specific media where the NPs would be used for process optimization.

Khademi-Azandehi and Moghadadam [71] compared the stability of AuNPs chemically synthesized and biosynthesized in different media (as synthesized and under physiological conditions simulated with pH 7.4 PBS solution). *Stachys lavandulifolia* Vahl extract maintained a more stable zeta potential value with changing solution, in contrast to sodium-citrate-mediated AuNPs. This improvement in the stability of AuNPs could be attributed to the presence of flavonoids and polyphenolic compounds that exist in plant extract [72]. These compounds increase the electrostatic forces. The stability of synthesized NPs increases in the colloidal solution when all particles are either positively or negatively charged; this increases the repulsion of particles from each other and prevents agglomeration or aggregation [73]. The zeta potential scan in the current study, which was performed on a wide scale (positive and negative scale), shows that all particles systematically bear a negative charge.

3.2.5. UV-Visible Spectroscopy

The purple color intensity, which was considered the first indicator for green synthesis of AuNPs, was monitored by UV-Vis spectroscopy to detect the maximum SPR (surface plasmon resonance). As shown, a single absorption peak is observed at $\lambda_{\max} = 530$ nm (Figure 4A); this SPR peak is typical of AuNPs and can be assigned to the free electron's collective oscillation in the conduction band [53,61]. Maliszewska et al. [54] also observed a single plasmon band at 522–523 nm. Muddapur et al. [26] reported that the appearance of a single SPR peak at a λ_{\max} in the range of 520–540 nm indicates the formation of tiny, monodispersed, and spherical AuNPs, which is consistent with TEM analysis. UV-Vis analysis (not shown) of the *Z. officinale* rhizome extract did not show any peak in this wavelength range; the SPR is thus characteristic of AuNPs. It is noteworthy that chemically mediated AuNPs have similar SPR values [74], and the purification of AuNPs with careful washing allows for the removal of the UV contributions of the residual plant extract (at low wavelengths), whereas the SPR peak remains unchanged at 530 nm. It is also noticeable that the width of the band remains relatively large, meaning that some residues are still present or that particles may partially aggregate.

3.2.6. FT-IR Spectroscopy

The functional groups in plant aqueous extract, as well as in plant-mediated AuNPs, were identified by Fourier transform infrared spectroscopy (FT-IR). As shown, the plant aqueous extract has nine peaks at wavenumbers of 3419, 2077, 1633, 1408, 1309, 1102, 1016, 700, and 515 cm^{-1} . These peaks are shifted after reacting with gold to produce AuNPs, in addition to the appearance of new peaks (Figure 4B and compiled assignments in the chart of phytosynthesized AuNPs in Table 2). The many functional groups present in plant aqueous extracts, such as amines, carbohydrates, proteins, and amino acids, can be involved in the reduction, capping, and stabilization of the as-formed AuNPs (based on the modification of their specific bands: shift or disappearance/appearance of new bands) [51] through the interaction of metal with various metabolites. This can be identified through the shift of some peaks or the changes in their relative intensities. Herein, changes

were observed in the peaks at 3419, 1633, 1408, 1102, 1016, 700, and 515 cm^{-1} , which were shifted to 3423, 1620, 1417, 1128, 1047, 780, and 513 cm^{-1} , respectively (with decreases in their relative intensities). This is consistent with previous observations [75,76]. It is noticeable that in the case of citrate-mediated synthesis of AuNPs, the FT-IR spectra show a much simpler profile with two main peaks corresponding to C=O symmetric stretching (at 1635 cm^{-1}) and C-H stretching vibration (at 1381 cm^{-1}). With the more complex composition of the ginger extract, many other functional groups representing the capping molecules that stabilize the AuNPs were also identified.

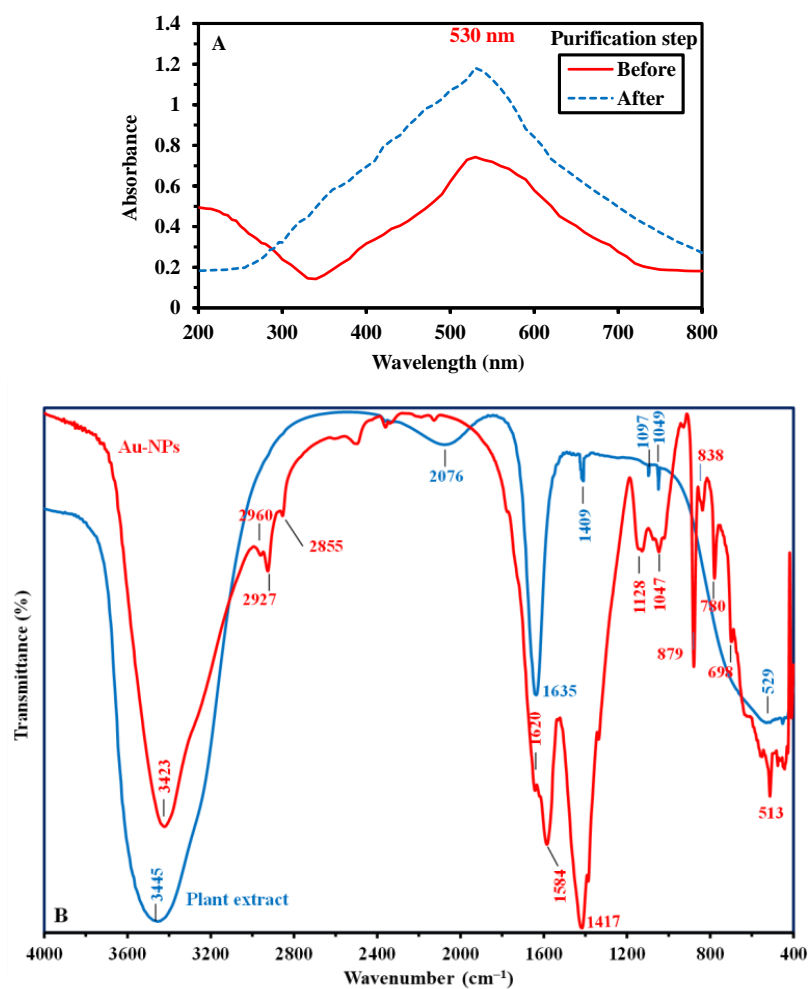


Figure 4. Characterization of materials. (A) UV-Vis spectrum of AuNPs (before and after purification); (B): FT-IR spectra of plant extract (aqueous extraction) and as-formed AuNPs.

Table 2. Assignment of peaks of plant aqueous extract and as-formed AuNPs.

| Vibration | Plant Extract | AuNPs | References |
|--|---------------|------------|------------|
| N-H/O-H stretching (overlapped) | 3419 | 3455 | [77] |
| C-H stretching of the aliphatic hydrocarbons | | 2927, 2855 | [78] |
| Aromatic compounds overlapped with $\nu(\text{C-O})$ | 2076 | | [71,79] |
| C=N, C=O of amide and N-H of the primary amine stretching (overlapped) | 1635 | 1620, 1584 | [78] |
| O-H, N-H of the secondary amine and C-H binding (overlapped) | 1409 | 1417 | [78] |
| $\nu(\text{C-O-C})$ carbohydrate, C-O stretching (overlapped) | 1097 | 1128 | [80] |
| C-N stretching | 1049 | 1047 | [81] |
| Aromatic C-H in plan bend | | 879, 838 | [82,83] |
| C-H Out of plane bending | | 780, 698 | [77] |
| C-S, C=S (overlapped) | 529 | 513 | [84] |

3.3. Antimicrobial Activity of AuNPs

The activity of AuNPs to control or inhibit the growth of potentially pathogenic microbes was investigated against *Bacillus subtilis*, *Staphylococcus aureus*, *Escherichia coli*, *Pseudomonas aeruginosa*, *Candida albicans*, and *Aspergillus brasiliensis*, as summarized in Figure 5A,B. Analysis of variance showed that the antimicrobial activity of synthesized AuNPs was dose-dependent. These results are compatible with those reported by Muddapur et al. [26] and Wani et al. [85], who showed that the antimicrobial activity of biosynthesized nanoparticles was dependent on various factors, such as size, shape, and concentration. Herein, the maximum zone of inhibition (ZOI) was reached at high AuNP concentrations ($200 \mu\text{g mL}^{-1}$): 18.7 ± 0.6 , 19.0 ± 1.0 , 21.3 ± 0.6 , 20.7 ± 0.6 , 17.7 ± 0.6 , and 16.7 ± 0.6 mm towards *B. subtilis*, *S. aureus*, *P. aeruginosa*, *E. coli*, *C. albicans*, and *A. brasiliensis*, respectively (Figure 5A,B). These inhibition zones decreased when the AuNP concentration was reduced to $100 \mu\text{g mL}^{-1}$ (16.3 ± 1.2 , 17.3 ± 0.6 , 19.3 ± 0.6 , 17.7 ± 1.2 , 15.7 ± 0.6 , and 14.3 ± 0.6 mm, respectively). With a dose of $50 \mu\text{g mL}^{-1}$, the ZOIs were reduced to 13.6 ± 0.6 , 14.7 ± 0.6 , 17.3 ± 0.6 , 16.3 ± 0.6 , 13.3 ± 0.5 , and 12.7 ± 0.6 , respectively. In a similar study, the antimicrobial and antifungal activity of AuNPs fabricated by the reaction of gold tetrachloride with the aqueous extract of *Annona muricata* increased with the dose of the antimicrobial agent [86]. Hence, Folorunso et al. reported that bacterial strains *Clostridium sporogenes*, *Enterococcus faecalis*, and *Klebsiella pneumonia* and fungal strains *A. flavus*, *F. oxysporium*, *P. camemeri*, and *C. albicans* were inhibited with percentages of 54, 46, 52, 31, 50, 66, and 42%, respectively, at a concentration of 4 mg L^{-1} . These values were slightly reduced to 50, 40, 49, 30, 45, 60, and 40%, respectively, when the concentration decreased to 2 mg L^{-1} . The maximum antibacterial activity of AuNPs formed by harnessing the metabolites of fresh leaves of *Pergularia daemia* was attained at $300 \mu\text{L mL}^{-1}$ against *S. aureus*, *E. coli*, and *P. aeruginosa*, with ZOIs of 16, 19, and 17 mm, respectively [87]. The incorporation of NPs into polymers or natural substances enhances their antibacterial activity. For instance, the coating of an amorphous carbon matrix with silver nanoparticles improves its antibacterial activity against *E. coli* and *S. aureus* [88]. In the current study, AuNPs exhibited promising antimicrobial activity with minimal cytotoxic effect against normal cells, supporting interest in their application in biomedicine. Consistently with this study, AgNPs synthesized by an aqueous extract of *Acanthospermum australe* exhibited antimicrobial activity toward various skin and soft tissue infection microbes with low cytotoxic activity against human normal cells [89]. Mussin et al. reported that this high antimicrobial activity is due to AgNPs rather than to the plant metabolites that coat the NP surfaces.

The effectiveness of infection control depends on the treatment strategy chosen; this also affects the evaluation of MIC (minimum inhibitory concentration) values [90]. In the current study, MIC values were evaluated based for the lowest concentration of AuNPs to inhibit microbial growth. Data analysis revealed that the MIC value was $25 \mu\text{g mL}^{-1}$ for *B. subtilis* and *A. brasiliensis*, with ZOIs of 11.3 ± 0.6 and 10.3 ± 0.6 mm, respectively. The MIC value was $6.25 \mu\text{g mL}^{-1}$ for *P. aeruginosa* and *E. coli* and $12.5 \mu\text{g mL}^{-1}$ for *S. aureus* and *C. albicans*, with ZOIs in the range of 9–11 mm (Figure 5A,B). Therefore, the antimicrobial activity of *Z. officinale*-based AuNPs against selected microorganisms can be ranked as follows: *P. aeruginosa* > *E. coli* > *S. aureus* > *B. subtilis* > *C. albicans* > *A. brasiliensis*.

The inhibitory effect of AuNPs is correlated with the chemical structure of Gram-positive and Gram-negative bacteria. In Gram-positive strains, the cell wall is composed of a thick layer of peptidoglycan (approximately 20–80 nm), compared with a thin layer (10 nm) in Gram-negative bacteria. Hence, the penetration of NPs into bacterial cell walls can be hindered, which explains the higher activity of synthesized AuNPs toward Gram-negative bacteria than against Gram-positive bacteria [1]. Another antimicrobial mechanism consists of the destruction of the cytoplasmic membrane because AuNP penetration leads to the inhibition of the selective permeability function [64]. After penetrating inside microbial cells, AuNPs react with cell components; nanoparticles inhibit the main functions, such as protein synthesis and DNA replications, and interact with the –SH group of amino acids,

ultimately causing cell death [91]. The release of toxic ions, including Au^+ , upon treatment of microbial strains with AuNPs is another inhibitory mechanism. This release occurs faster at high concentrations and with smaller NPs; this mechanism could explain the high activity of synthesized AuNPs at high concentrations, as reported previously [1]. Upon bacterial treatment, released Au^+ ions cover cell organelles and cell membranes through a reaction with -SH groups to form Au-SH groups, which, in turn, cause protein coagulation [92]. In addition, the formation of this new group (Au-SH) can involve the inhibition of the cell wall synthetase pathway, the disruption of microbial respiration, and the blocking of active transport chains [93]. Finally, ROS (reactive oxygen species)-mediated oxidative stress strongly contributes to the inhibitory mechanism [28]. The presence of NPs inside the cells enhances the production of free radicals, such as O_2^- , H_2O_2 , and $\bullet\text{OH}$ [93]. Under normal conditions, bacterial cells have the capacity to inhibit these toxic free or activated ions, whereas under stress (such as in the presence of NPs), the cells lose their potential to scavenge these ions. This blockage causes oxidative stress and redox imbalance, with ultimate cell death [94]. The disruption of sterol profiles in *Candida* cell walls occurs through the inhibition of the ergosterol pathway by NPs; this is considered the main mechanism for the growth inhibition of *C. albicans*. Indeed, sterols are crucial components responsible for *Candida* cell wall rigidity, integrity, homogeneity, and fluidity [95,96].

3.4. Antioxydant Activity of AuNPs

Oxidative stress is associated with many diseases, including cancer, high blood pressure, diabetes, and atherosclerosis. Interestingly, the oxidation of substrates can be slowed or prevented by low concentrations of antioxidants (organic chemical compounds) [40]. Metal nanoparticles have been reported as an efficient antioxidant against DPPH (prevalent nitrogen-centered free radical) [6]. Accordingly, a DPPH assay was used herein to examine the prospective properties of *Z. officinale*-derived AuNPs as antioxidants. According to the results summarized in Figure 6, the DPPH scavenging activity of AuNPs has values significantly higher than the levels recorded for standard ascorbic acid ($p \leq 0.05$). Moreover, the free radical-scavenging potential of the phytoderived AuNPs is dose-dependent; antioxidant activity increases with concentration. At high concentrations (i.e., $1000 \mu\text{g mL}^{-1}$), synthesized AuNPs displayed scavenging activity with an efficiency of $87.6 \pm 0.5\%$ compared to ascorbic acid as a control (which showed scavenging activity percentages of $97.3 \pm 0.2\%$, Figure 6).

Analysis of variance clearly shows that the scavenging activity decreases with reduced concentration. For instance, the scavenging activity percentages were recorded at values of 82.5 ± 1.4 , 77.2 ± 2.2 , 62.7 ± 2.9 , and $31.8 \pm 3.1\%$ at concentrations of 500, 250, 62.5, and $1.9 \mu\text{g mL}^{-1}$ respectively, as compared to a control, with percentages of 94.1 ± 0.2 , 87.8 ± 0.1 , 75.1 ± 0.2 , and $37.5 \pm 1.3\%$ at the same concentration for ascorbic acid. The IC_{50} values for phytosynthesized AuNPs that correspond to a scavenging efficiency of 50% were calculated. Data analysis shows that the IC_{50} value for AuNPs was close to $16 \mu\text{g mL}^{-1}$, compared with a value of $12.8 \mu\text{g mL}^{-1}$ for ascorbic acid. In agreement with our results, *Sargassum longifolium*-mediated AuNPs displayed considerable antioxidant activity against H_2O_2 ($25 \mu\text{g mL}^{-1}$) and DPPH free radicals ($20\text{--}30 \mu\text{g mL}^{-1}$) [44]. Similarly, AuNPs prepared from plant extract (*Physalis minima*) showed efficient scavenging activity against DPPH in a dose-dependent manner; this activity was attributed to their catalytic properties and the large surface area of AuNPs, which enhances their antioxidant capacity [25]. It was proposed that the antioxidant activity of biologically manufactured AuNPs may be due to their ability to transfer hydrogen or an electron (at the atomic level) to the free radical (DPPH \bullet) and convert it to stable DPPH-H [97]. Similarly, the phytoengineered AuNPs from the aqueous extract of *Acalypha indica* showed efficient DPPH scavenging potency, and the IC_{50} value was evaluated as $16.25 \mu\text{g mL}^{-1}$ [98], which is consistent with the current study. Apart from the contribution of AuNPs, the presence of plant secondary metabolites, such as sesquiterpenes, phenolic, and flavonoid compounds (which play a role in the synthesis and the capping of AuNPs), may also assist the antioxidant activity of nanoparticles [99].

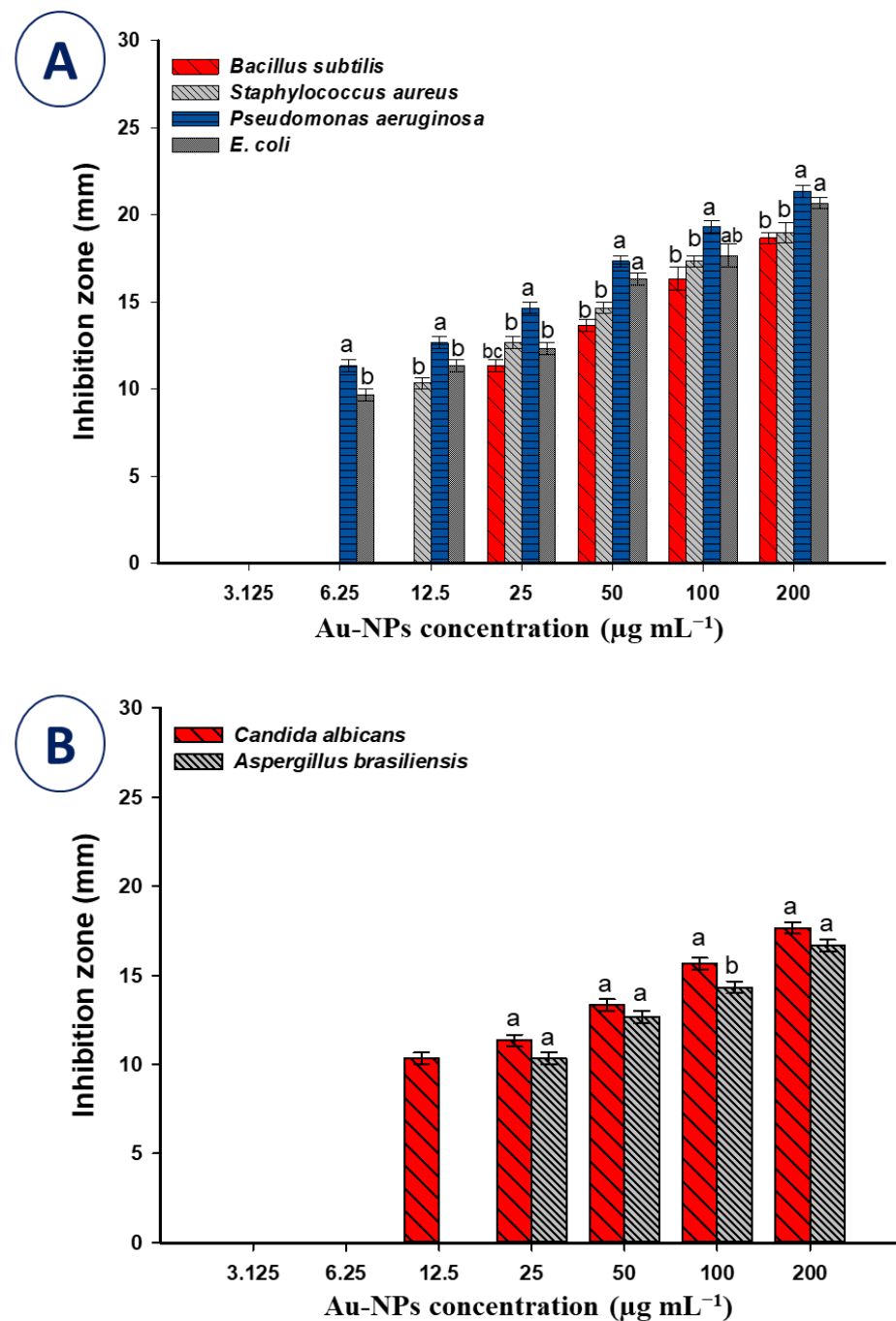


Figure 5. Antimicrobial activity of *Z. officinale*-mediated green synthesis of AuNPs against (A) Gram-positive and Gram-negative bacteria, and (B) unicellular fungi, and multicellular fungi. Data are presented as average value \pm SD ($n = 3$). Different letters on the bars at the same concentration indicate that the mean values are significantly different (at $p \leq 0.05$).

Gold nanoparticles have been reported to have a cytotoxic effect through induction of oxidative stress [100,101]. However, in this study, green synthesized AuNPs showed high antioxidant activity. This difference is associated with the role of mitochondria in the induced production of free radicals. The oxidative stress production by the action of nanoparticles is influenced by many factors, including non-cellular factors, such as the presence of metals, the size and surface area of the nanoparticles, concentrations, and method of synthesis, in addition to cellular factors, such as the interaction of the nanoparticles with cells [102,103].

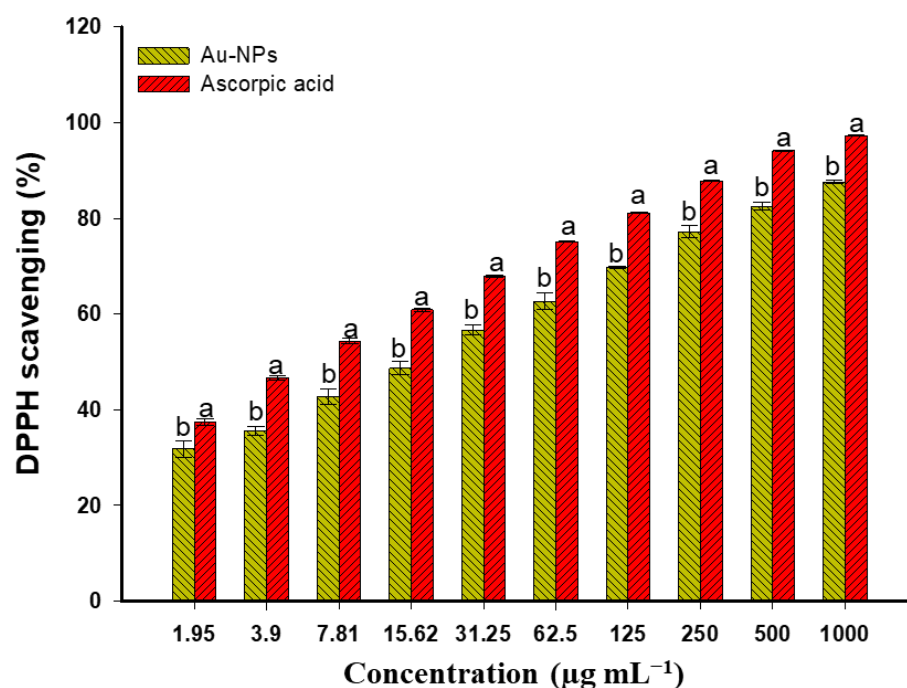


Figure 6. Antioxidant activity of plant-based AuNPs measured by DPPH method at different concentrations compared to ascorbic acid. Data show average values \pm SD ($n = 3$). Different letters on the bars at the same concentration indicate that the mean values are significantly different (at $p \leq 0.05$).

3.5. Cytotoxicity Assay of AuNPs

The development of therapeutic nanotechnology using nanogold, especially in diagnosis and treatment in oncology, requires numerous toxicological examinations to detect the appropriate dosing for patient safety [104,105]. Herein, an MTT assay was used to evaluate the nanotoxicological properties of *Z. officinale*-induced AuNPs against normal and tumor cell lines. Consistent with previous studies, AuNPs displayed powerful cytotoxicity against cancerous and normal cells in a dose-dependent mode [106]. These findings can be correlated to the microscopic changes and cytotoxic effects of AuNPs toward the PC12 cancer cell line, which were both concentration-dependent [107]. The cancer cell lines HepG2 and MCF7 lose approximately 94.8% and 70% of their viability, respectively, after treatment with 500 $\mu\text{g mL}^{-1}$, whereas the normal OEC cell line only loses about 50% of its viability at the same concentration (Figure 7). On the other hand, the normal and cancer cell lines recover their viability percentages with concentrations reduced to $99.4 \pm 1.8\%$, 51.8 ± 0.9 , and $83.9 \pm 0.5\%$ for OEC, HepG2, and MCF7, respectively, at a concentration of 125 $\mu\text{g mL}^{-1}$. This indicates that the phytosynthesized AuNPs are more active against hepatocellular carcinoma (HepG2) than adenocarcinoma (MCF7), with negligible activity against normal oral epithelial cells at concentrations of 250 and 125 $\mu\text{g mL}^{-1}$ (Figure 7).

Analysis of variance showed that the maximum antiproliferative effect was observed for the hepatocellular carcinoma HepG2 cells, with an IC_{50} value of $131.9 \pm 9.34 \mu\text{g mL}^{-1}$, whereas the AuNP concentration required for 50% morbidity (IC_{50}) of adenocarcinoma MCF7 cells reached $288.23 \pm 31.39 \mu\text{g mL}^{-1}$. In contrast, the value of IC_{50} for the normal oral epithelial OEC cells was $487.612 \pm 3.53 \mu\text{g/mL}$ (Figure 7). The significant difference in IC_{50} values between tested cancerous and normal cells may represent a safe therapeutic window to determine doses and spare patients from harmful side effects.

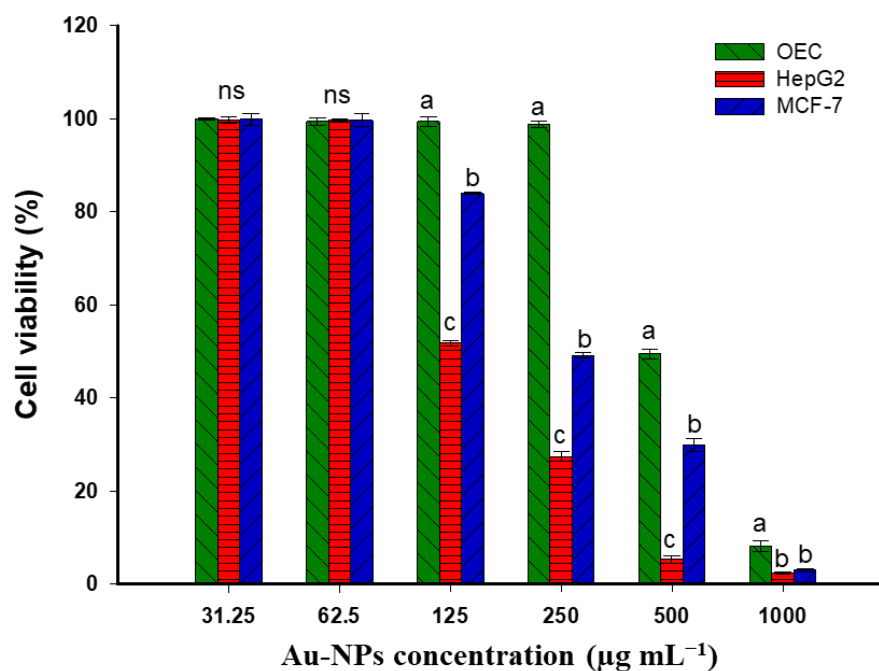


Figure 7. In vitro cytotoxic efficacy of phytosynthesized AuNPs against a normal cell line (OEC) and cancer cell lines (HepG2 and MCF7) evaluated by MTT assay method. Data represent average values \pm SD ($n = 3$). Different letters on the bars at the same concentration indicated that the mean values are significantly different (at $p \leq 0.05$); ns, the mean values are non-significantly different.

Similarly, Chang et al. [108] reported the efficient toxicological properties of phytofabricated AuNPs against the lymphoblastic leukemia cell lines Molt-3 and TALL-104, with IC_{50} values of 329 and 381 $\mu\text{g}/\text{mL}$, respectively. On the other hand, AuNPs derived from Parsley leaf extract reduced the viability of the human colorectal cell line (CO-II) at a low concentration ($IC_{50} = 56.83 \text{ g}/\text{mL}$); this enhanced cytotoxicity could be attributed to the free radicals generated by nanoparticles. In addition, the tiny size of nanoparticles contributes to the destruction of the membrane of cancer cells [109]. Biogenic gold nanoparticles were found to be excellent candidates for biomedical applications and safe for a normal cell line but toxic to cancer cells (MDA-MB-231) [110]. Jeyarani et al. correlated observed morphological changes with cell apoptosis induced by AuNPs. Steckiewicz et al. [105] commented that AuNPs reduced the viability of breast adenocarcinoma and hepatocellular carcinoma. The characteristic nanotoxicological potential was attributed to several possible mechanisms and causes associated with the shape of AuNPs, incubation time, size, concentration, surface functionalization, fabrication method, and the type of treated cells.

Figure 8 depicts the microscopic observation of normal and cancer cell lines after treatment with various concentrations of AuNPs. The synthesized active compound affects the monolayer sheets of the normal cells at high concentrations (i.e., 1000 $\mu\text{g mL}^{-1}$), whereas normal shape is recovered by lowering the dose to or below 500 $\mu\text{g mL}^{-1}$. On the other hand, the morphological shape of cancer cell lines is highly affected by lower nanogold concentrations. The most significant morphological changes concern the integrity of the monolayer sheets of epithelial cells that are damaged. After treating the cell suspension with different concentrations of AuNPs, their aspect changes with the formation of shrunk, buoyant, grainy, and spherical cells. These morphological changes could be attributed to the production of ROS due to the entrance of NPs into mammalian cells through endocytosis. ROS can damage the mitochondrial membrane and enhance the apoptotic pathways, ultimately leading to cell death or cell morphological changes [111,112]. Taha [57] also reported the possibility of AuNPs affecting the nuclei of cells (in the case of a human cervical cancer cell line, HeLa); by damaging nuclei, the NPs affect the DNA and cause S-phase arrest (affecting apoptosis through an increase in Sub-G1).

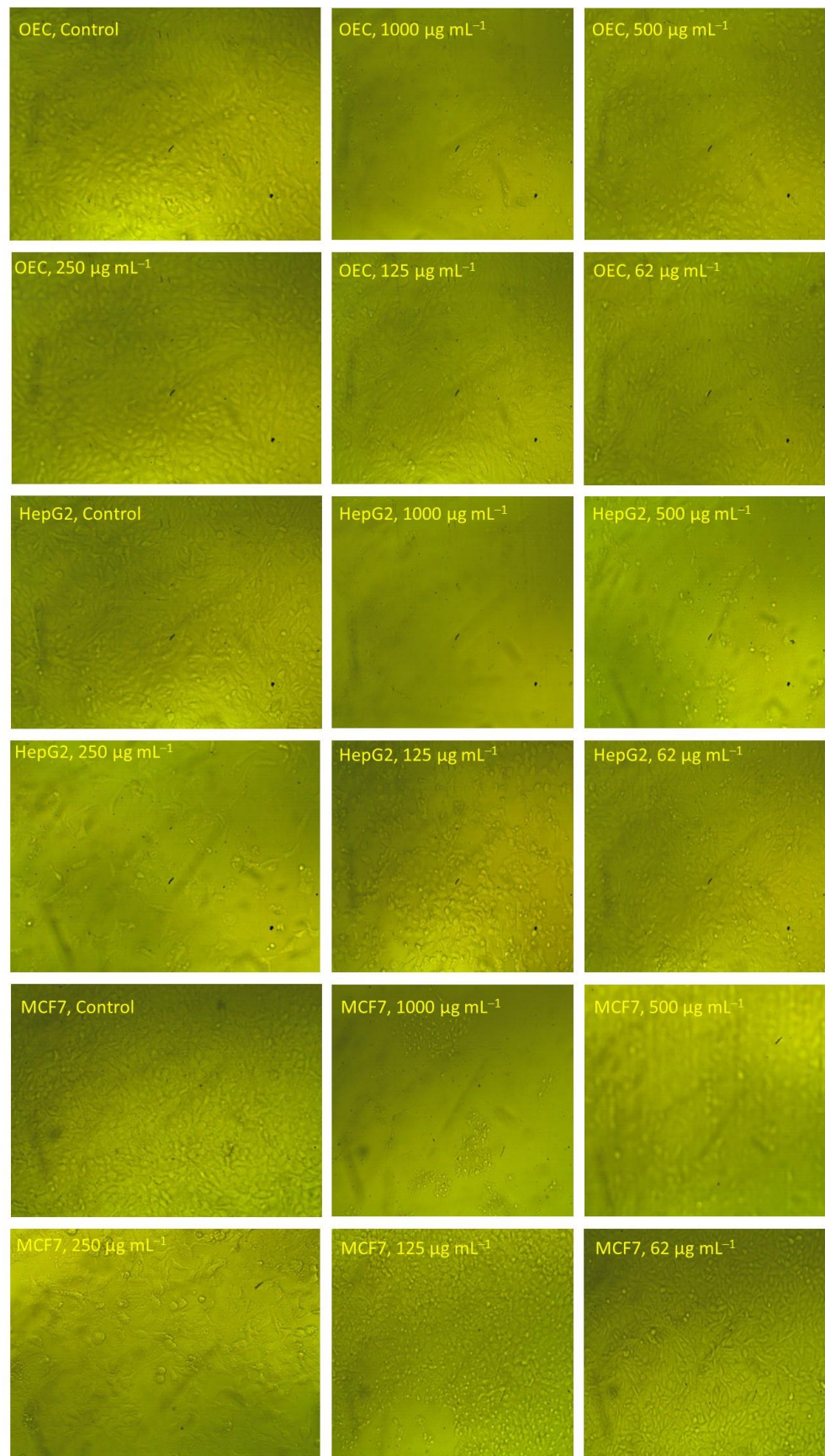


Figure 8. Morphological changes of normal cell lines (OEC) and cancer cell lines (HepG2 and MCF7) after treatment with various concentrations of phytosynthesized AuNPs.

4. Conclusions

Herein, AuNPs were successfully synthesized by reaction of the aqueous extract of *Zingiber officinale* rhizome with chloroauric acid; this was confirmed by color change (from colorless to purple color). A UV-Vis spectrophotometer showed maximum SPR at 530 nm. TEM showed spherical nanoparticles with sizes of 5–53 nm (average nanoparticle size: 15.11 ± 8.5 nm). XRD confirmed the crystalline nature of the material. FT-IR spectroscopy enabled identification of the main functional groups in the plant extract and synthesized AuNPs. The high stability of nanoparticles in the colloidal solution was confirmed by DLS and zeta potential characterizations. Biological activities, including antimicrobial activity, as well as antioxidant and in vitro cytotoxic efficacy, were investigated and found to be dose-dependent. The synthesized AuNPs displayed high activity against pathogenic microbes, high antioxidant activity, and target-oriented cytotoxicity toward cancer cell lines (compared to negligible cytotoxicity against normal cell lines). Overall, *Zingiber officinale* extract shows high potential to produce highly active AuNPs, with potential for various biomedical applications.

Author Contributions: Conceptualization, A.F., A.M.E., E.G. and S.E.-D.H.; methodology, A.F., A.M.E., M.F.H. and S.E.-D.H.; software, A.F., A.M.E., E.G., M.F.H. and S.E.-D.H.; validation, A.F., E.G. and S.E.-D.H.; formal analysis, A.F., A.M.E., E.G., M.F.H. and S.E.-D.H.; investigation, A.F., A.M.E., D.H.M.A., D.E.-H. and S.E.-D.H.; resources, A.F., A.M.E., D.H.M.A., D.E.-H. and S.E.-D.H.; data curation, A.F., A.M.E. and E.G.; writing—original draft preparation, A.F., A.M.E. and S.E.-D.H.; writing—review and editing, A.F., E.G. and M.F.H.; visualization, A.F. and A.M.E.; supervision, A.F., E.G. and S.E.-D.H.; project administration, A.F. and E.G.; funding acquisition, A.F., M.F.H., D.H.M.A. and D.E.-H. All authors have read and agreed to the published version of the manuscript.

Funding: This research received no external funding.

Institutional Review Board Statement: Not applicable.

Informed Consent Statement: Not applicable.

Data Availability Statement: The data presented in this study are available upon request from the corresponding authors.

Acknowledgments: The authors extend their appreciation to the Botany and Microbiology Department, Faculty of Science, Al-Azhar University, Cairo, Egypt, for the great support in the achievement and publication of this research work. Furthermore, the authors acknowledge the support from Princess Nourah bint Abdulrahman University Researchers Supporting (project number PNURSP2022R15), Princess Nourah bint Abdulrahman University, Riyadh, Saudi Arabia.

Conflicts of Interest: The authors declare no conflict of interest.

References

1. Gu, X.; Xu, Z.X.; Gu, L.P.; Xu, H.Y.; Han, F.X.; Chen, B.; Pan, X.J. Preparation and antibacterial properties of gold nanoparticles: A review. *Environ. Chem. Lett.* **2021**, *19*, 167–187. [[CrossRef](#)]
2. Bukowski, K.; Kciuk, M.; Kontek, R. Mechanisms of multidrug resistance in cancer chemotherapy. *Int. J. Mol. Sci.* **2020**, *21*, 3233. [[CrossRef](#)]
3. Miller, K.D.; Nogueira, L.; Mariotto, A.B.; Rowland, J.H.; Yabroff, K.R.; Alfano, C.M.; Jemal, A.; Kramer, J.L.; Siegel, R.L. Cancer treatment and survivorship statistics, 2019. *CA Cancer J. Clin.* **2019**, *69*, 363–385. [[CrossRef](#)] [[PubMed](#)]
4. Fouda, A.; Eid, A.M.; Abdelkareem, A.; Said, H.A.; El-Belely, E.F.; Alkhalifah, D.H.M.; Alshallash, K.S.; Hassan, S.E.D. Phyco-synthesized zinc oxide nanoparticles using marine macroalgae, *Ulva fasciata* Delile, characterization, antibacterial activity, photocatalysis, and tanning wastewater treatment. *Catalysts* **2022**, *12*, 756. [[CrossRef](#)]
5. Palani, G.; Arputhalatha, A.; Kannan, K.; Lakkaboyana, S.K.; Hanafiah, M.M.; Kumar, V.; Marella, R.K. Current trends in the application of nanomaterials for the removal of pollutants from industrial wastewater treatment-A review. *Molecules* **2021**, *26*, 2799. [[CrossRef](#)] [[PubMed](#)]
6. Bhakya, S.; Muthukrishnan, S.; Sukumaran, M.; Muthukumar, M. Biogenic synthesis of silver nanoparticles and their antioxidant and antibacterial activity. *Appl. Nanosci.* **2016**, *6*, 755–766. [[CrossRef](#)]
7. Fouda, A.; Al-Otaibi, W.A.; Saber, T.; AlMotwaa, S.M.; Alshallash, K.S.; Elhady, M.; Badr, N.F.; Abdel-Rahman, M.A. Antimicrobial, antiviral, and in-vitro cytotoxicity and mosquitocidal activities of *Portulaca oleracea*-based green synthesis of selenium nanoparticles. *J. Funct. Biomater.* **2022**, *13*, 157. [[CrossRef](#)]

8. Datta, D.; Deepak, K.S.; Das, B. Progress in the synthesis, characterisation, property enhancement techniques and application of gold nanoparticles: A review. *MRS Commun.* **2022**, *12*, 700–715. [[CrossRef](#)]
9. Chen, X.Y.; Zhao, X.; Wang, G.X. Review on marine carbohydrate-based gold nanoparticles represented by alginate and chitosan for biomedical application. *Carbohydr. Polym.* **2020**, *244*, 116311. [[CrossRef](#)]
10. Firdhouse, M.J.; Lalitha, P. Biogenic green synthesis of gold nanoparticles and their applications—A review of promising properties. *Inorg. Chem. Commun.* **2022**, *143*, 109800. [[CrossRef](#)]
11. Heinemann, M.G.; Rosa, C.H.; Rosa, G.R.; Dias, D. Biogenic synthesis of gold and silver nanoparticles used in environmental applications: A review. *Trends Environ. Anal. Chem.* **2021**, *30*, e00129. [[CrossRef](#)]
12. Gour, A.; Jain, N.K. Advances in green synthesis of nanoparticles. *Artif. Cells Nanomed. Biotechnol.* **2019**, *47*, 844–851. [[CrossRef](#)] [[PubMed](#)]
13. Yazdani, M.; Rostamzadeh, P.; Rahbar, M.; Alam, M.; Abbasi, K.; Tahmasebi, E.; Tebyaniyan, H.; Ranjbar, R.; Seifalian, A.; Yazdani, A. The potential application of green-synthesized metal nanoparticles in dentistry: A comprehensive review. *Bioinorg. Chem. Appl.* **2022**, *2022*, 2311910. [[CrossRef](#)] [[PubMed](#)]
14. Akintelu, S.A.; Olugbeko, S.C.; Folorunso, A.S. A review on synthesis, optimization, characterization and antibacterial application of gold nanoparticles synthesized from plants. *Int. Nano Lett.* **2020**, *10*, 237–248. [[CrossRef](#)]
15. Burlacu, E.; Tanase, C.; Coman, N.A.; Berta, L. A review of bark-extract-mediated green synthesis of metallic nanoparticles and their applications. *Molecules* **2019**, *24*, 4354. [[CrossRef](#)] [[PubMed](#)]
16. Dash, S.S.; Sen, I.K.; Dash, S.K. A review on the plant extract mediated green syntheses of gold nanoparticles and its anti-microbial, anti-cancer and catalytic applications. *Int. Nano Lett.* **2022**, *12*, 47–66. [[CrossRef](#)]
17. Hano, C.; Abbasi, B.H. Plant-based green synthesis of nanoparticles: Production, characterization and applications. *Biomolecules* **2022**, *12*, 31. [[CrossRef](#)]
18. Fouda, A.; Hassan, S.E.D.; Eid, A.M.; Abdel-Rahman, M.A.; Hamza, M.F. Light enhanced the antimicrobial, anticancer, and catalytic activities of selenium nanoparticles fabricated by endophytic fungal strain, *Penicillium crustosum* EP-1. *Sci. Rep.* **2022**, *12*, 11834. [[CrossRef](#)]
19. Kaur, K.; Thombre, R. Chapter 1—Nanobiotechnology: Methods, applications, and future prospects. In *Nanobiotechnology*; Ghosh, S., Webster, T.J., Eds.; Elsevier: Amsterdam, The Netherlands, 2021; pp. 1–20. [[CrossRef](#)]
20. Timoszyk, A. A review of the biological synthesis of gold nanoparticles using fruit extracts: Scientific potential and application. *Bull. Mater. Sci.* **2018**, *41*, 154. [[CrossRef](#)]
21. Dhumale, V.A.; Gangwar, R.K.; Pande, N. Importance of gold nanoparticles for detection of toxic heavy metal ions and vital role in biomedical applications. *Mater. Res. Innov.* **2021**, *25*, 354–362. [[CrossRef](#)]
22. Dheyab, M.A.; Aziz, A.A.; Khaniabadi, P.M.; Jameel, M.S.; Oladzadabbasabadi, N.; Mohammed, S.A.; Abdullah, R.S.; Mehrdel, B. Monodisperse gold nanoparticles: A review on synthesis and their application in modern medicine. *Int. J. Mol. Sci.* **2022**, *23*, 7400. [[CrossRef](#)] [[PubMed](#)]
23. Piktel, E.; Suprewicz, L.; Depciuch, J.; Chmielewska, S.; Sklodowski, K.; Daniluk, T.; Krol, G.; Kolat-Brodecka, P.; Bijak, P.; Pajor-Swierzy, A.; et al. Varied-shaped gold nanoparticles with nanogram killing efficiency as potential antimicrobial surface coatings for the medical devices. *Sci. Rep.* **2021**, *11*, 12546. [[CrossRef](#)]
24. Paradowska, E.; Studzinska, M.; Jablonska, A.; Lozovski, V.; Rusinchuk, N.; Mukha, I.; Vitiuk, N.; Lesnikowski, Z.J. Antiviral effect of nonfunctionalized gold nanoparticles against Herpes Simplex Virus Type-1 (HSV-1) and possible contribution of near-field interaction mechanism. *Molecules* **2021**, *26*, 5960. [[CrossRef](#)] [[PubMed](#)]
25. Sekar, V.; Al-Ansari, M.M.; Narenkumar, J.; Al-Humaid, L.; Arunkumar, P.; Santhanam, A. Synthesis of gold nanoparticles (AuNPs) with improved anti-diabetic, antioxidant and anti-microbial activity from *Physalis minima*. *J. King Saud Univ. Sci.* **2022**, *34*, 102197. [[CrossRef](#)]
26. Muddapur, U.M.; Alshehri, S.; Ghoneim, M.M.; Mahnashi, M.H.; Alshahrani, M.A.; Khan, A.A.; Iqbal, S.M.S.; Bahafi, A.; More, S.S.; Shaikh, I.A.; et al. Plant-based synthesis of gold nanoparticles and theranostic applications: A review. *Molecules* **2022**, *27*, 1391. [[CrossRef](#)] [[PubMed](#)]
27. Okkeh, M.; Bloise, N.; Restivo, E.; De Vita, L.; Pallavicini, P.; Visai, L. Gold nanoparticles: Can they be the next magic bullet for multidrug-resistant bacteria? *Nanomaterials* **2021**, *11*, 312. [[CrossRef](#)] [[PubMed](#)]
28. Mishra, A.; Pradhan, D.; Halder, J.; Biswasroy, P.; Rai, V.K.; Dubey, D.; Kar, B.; Ghosh, G.; Rath, G. Metal nanoparticles against multi-drug-resistance bacteria. *J. Inorg. Biochem.* **2022**, *237*, 111938. [[CrossRef](#)]
29. Rasool, N.; Saeed, Z.; Pervaiz, M.; Ali, F.; Younas, U.; Bashir, R.; Bukhari, S.M.; Khan, R.R.M.; Jelani, S.; Sikandar, R. Evaluation of essential oil extracted from ginger, cinnamon and lemon for therapeutic and biological activities. *Biocatal. Agric. Biotechnol.* **2022**, *44*, 102470. [[CrossRef](#)]
30. Halimin, N.M.S.; Abdullah, M.O.; Wahab, N.A.; Junin, R.; Husaini, A.; Agi, A. Oil extracts from fresh and dried *Iban* ginger. *Chin. J. Anal. Chem.* **2022**, *50*, 100119. [[CrossRef](#)]
31. Deng, X.H.; Chen, D.D.; Sun, X.J.; Dong, J.C.; Huang, J.H. Effects of ginger extract and its major component 6-gingerol on anti-tumor property through mitochondrial biogenesis in CD8(+) T cells. *J. Food Sci.* **2022**, *87*, 3307–3317. [[CrossRef](#)]
32. Zhou, X.; Afzal, S.; Wohlmuth, H.; Munch, G.; Leach, D.; Low, M.; Li, C.G. Synergistic anti-inflammatory activity of ginger and turmeric extracts in inhibiting lipopolysaccharide and interferon-gamma-induced proinflammatory mediators. *Molecules* **2022**, *27*, 3877. [[CrossRef](#)] [[PubMed](#)]

33. Martín Ortega, A.M.; Segura Campos, M.R. Chapter 5—Medicinal Plants and Their Bioactive Metabolites in Cancer Prevention and Treatment. In *Bioactive Compounds*; Campos, M.R.S., Ed.; Woodhead Publishing: Sawston, UK, 2019; pp. 85–109. [[CrossRef](#)]
34. Shahin, H.D.H.; Sultana, R.; Farooq, J.; Taj, T.; Khaiser, U.F.; Alanazi, N.S.A.; Alshammari, M.K.; Alshammari, M.N.; Alsubaie, F.H.; Asdaq, S.M.B.; et al. Insights into the uses of traditional plants for diabetes nephropathy: A review. *Curr. Issues Mol. Biol.* **2022**, *44*, 2887–2902. [[CrossRef](#)] [[PubMed](#)]
35. Yasmin, A.R.; Chia, S.L.; Looi, Q.H.; Omar, A.R.; Noordin, M.M.; Ideris, A. Chapter 7—Herbal extracts as antiviral agents. In *Feed Additives*; Florou-Paneri, P., Christaki, E., Giannenas, I., Eds.; Academic Press: Cambridge, MA, USA, 2020; pp. 115–132. [[CrossRef](#)]
36. Abbas, A.H.; Fairouz, N.Y. Characterization, biosynthesis of copper nanoparticles using ginger roots extract and investigation of its antibacterial activity. In Proceedings of the International Conference on Recent Advances in Mechanical Engineering and Nanomaterials (ICRAMEN), Pune, India, 20 February 2022; pp. 908–913.
37. Ramzan, M.; Karobari, M.I.; Heboyan, A.; Mohamed, R.N.; Mustafa, M.; Basheer, S.N.; Desai, V.; Batool, S.; Ahmed, N.; Zeshan, B. Synthesis of silver nanoparticles from extracts of wild ginger (*Zingiber zerumbet*) with antibacterial activity against selective multidrug resistant oral bacteria. *Molecules* **2022**, *27*, 2007. [[CrossRef](#)] [[PubMed](#)]
38. Yadi, M.; Azizi, M.; Dianat-Moghadam, H.; Akbarzadeh, A.; Abyadeh, M.; Milani, M. Antibacterial activity of green gold and silver nanoparticles using ginger root extract. *Bioprocess Biosyst. Eng.* **2022**, *45*, 1905–1917. [[CrossRef](#)] [[PubMed](#)]
39. Lee, K.X.; Shameli, K.; Miyake, M.; Kuwano, N.; Khairudin, N.B.B.A.; Mohamad, S.E.B.; Yew, Y.P. Green synthesis of gold nanoparticles using aqueous extract of *Garcinia mangostana* fruit peels. *J. Nanomater.* **2016**, *2016*, 8489094. [[CrossRef](#)]
40. Al-Radadi, N.S. Biogenic proficient synthesis of (Au-NPs) via aqueous extract of Red Dragon Pulp and seed oil: Characterization, antioxidant, cytotoxic properties, anti-diabetic anti-inflammatory, anti-Alzheimer and their anti-proliferative potential against cancer cell lines. *Saudi J. Biol. Sci.* **2022**, *29*, 2836–2855. [[CrossRef](#)]
41. Al Saqr, A.; Khafagy, E.-S.; Alalaiwe, A.; Aldawsari, M.E.; Alshahrani, S.M.; Anwer, M.K.; Khan, S.; Abu Lila, A.S.; Arab, H.H.; Hegazy, W.A.H. Synthesis of gold nanoparticles by using green machinery: Characterization and in vitro toxicity. *Nanomaterials* **2021**, *11*, 808. [[CrossRef](#)]
42. Holzwarth, U.; Gibson, N. The Scherrer equation versus the ‘Debye-Scherrer equation’. *Nat. Nanotechnol.* **2011**, *6*, 534. [[CrossRef](#)]
43. Humphries, R.M.; Ambler, J.; Mitchell, S.L.; Castanheira, M.; Dingle, T.; Hindler, J.A.; Koeth, L.; Sei, K.; Standardization, C.M.D. CLSI methods development and standardization working group best practices for evaluation of antimicrobial susceptibility tests. *J. Clin. Microbiol.* **2018**, *56*, e01934-17. [[CrossRef](#)]
44. Rajeshkumar, S.; Parameswari, R.P.; Jayapriya, J.; Tharani, M.; Ali, H.; Aljarba, N.H.; Alkahtani, S.; Alarifi, S. Apoptotic and antioxidant activity of gold nanoparticles synthesized using marine brown seaweed: An in vitro study. *Biomed Res. Int.* **2022**, *2022*, 5746761. [[CrossRef](#)]
45. Fouda, A.; Hassan, S.E.-D.; Eid, A.M.; Awad, M.A.; Althumayri, K.; Badr, N.F.; Hamza, M.F. Endophytic bacterial strain, *Brevibacillus brevis*-mediated green synthesis of copper oxide nanoparticles, characterization, antifungal, in vitro cytotoxicity, and larvicidal activity. *Green Process. Synth.* **2022**, *11*, 931–950. [[CrossRef](#)]
46. Chambers, J.M.; Cleveland, W.S.; Kleiner, B.; Tukey, P.A. *Graphical Methods for Data Analysis*; Wadsworth International Group: Belmont, CA, USA, 1983.
47. Zhang, D.; Ma, X.-L.; Gu, Y.; Huang, H.; Zhang, G.-W. Green synthesis of metallic nanoparticles and their potential applications to treat cancer. *Front. Chem.* **2020**, *8*, 799. [[CrossRef](#)] [[PubMed](#)]
48. Bharadwaj, K.K.; Rabha, B.; Pati, S.; Sarkar, T.; Choudhury, B.K.; Barman, A.; Bhattacharjya, D.; Srivastava, A.; Baishya, D.; Edinur, H.A.; et al. Green synthesis of gold nanoparticles using plant extracts as beneficial prospect for cancer theranostics. *Molecules* **2021**, *26*, 6389. [[CrossRef](#)]
49. Liu, H.; Yang, H.; Zhao, T.; Lin, C.; Li, Y.; Zhang, X.; Ye, Y.; Liao, J. Combined metabolome and transcriptome analyses of young, mature, and old rhizome tissues of *Zingiber officinale* Roscoe. *Front. Genet.* **2021**, *12*, 795201. [[CrossRef](#)] [[PubMed](#)]
50. Mao, Q.-Q.; Xu, X.-Y.; Cao, S.-Y.; Gan, R.-Y.; Corke, H.; Beta, T.; Li, H.-B. Bioactive compounds and bioactivities of ginger (*Zingiber officinale* Roscoe). *Foods* **2019**, *8*, 185. [[CrossRef](#)]
51. Elia, P.; Zach, R.; Hazan, S.; Kolusheva, S.; Porat, Z.E.; Zeiri, Y. Green synthesis of gold nanoparticles using plant extracts as reducing agents. *Int. J. Nanomed.* **2014**, *9*, 4007–4021. [[CrossRef](#)]
52. ElMitwalli, O.S.; Barakat, O.A.; Daoud, R.M.; Akhtar, S.; Henari, F.Z. Green synthesis of gold nanoparticles using cinnamon bark extract, characterization, and fluorescence activity in Au/eosin Y assemblies. *J. Nanoparticle Res.* **2020**, *22*, 309. [[CrossRef](#)]
53. Parial, D.; Patra, H.K.; Roychoudhury, P.; Dasgupta, A.K.; Pal, R. Gold nanorod production by cyanobacteria—a green chemistry approach. *J. Appl. Phycol.* **2012**, *24*, 55–60. [[CrossRef](#)]
54. Maliszewska, I.; Wanarska, E.; Thompson, A.C.; Samuel, I.D.W.; Matczyszyn, K. Biogenic gold nanoparticles decrease methylene blue photobleaching and enhance antimicrobial photodynamic therapy. *Molecules* **2021**, *26*, 623. [[CrossRef](#)]
55. Huang, Q.H.; Luo, A.H.; Jiang, L.J.; Zhou, Y.; Yang, Y.T.; Liu, Q.; Zhang, C.F. Disinfection efficacy of green synthesized gold nanoparticles for medical disinfection applications. *Afr. Health Sci.* **2019**, *19*, 1441–1448. [[CrossRef](#)]
56. Li, S.Q.; Al-Misned, F.A.; El-Serehy, H.A.; Yang, L.L. Green synthesis of gold nanoparticles using aqueous extract of *Mentha Longifolia* leaf and investigation of its anti-human breast carcinoma properties in the in vitro condition. *Arab. J. Chem.* **2021**, *14*, 102931. [[CrossRef](#)]

57. Taha, R.H. Green synthesis of silver and gold nanoparticles and their potential applications as therapeutics in cancer therapy; a review. *Inorg. Chem. Commun.* **2022**, *143*, 109610. [[CrossRef](#)]
58. Patra, J.K.; Baek, K.H. Green nanobiotechnology: Factors affecting synthesis and characterization techniques. *J. Nanomater.* **2014**, *2014*, 417305. [[CrossRef](#)]
59. Hebie, S.; Kokoh, K.B.; Servat, K.; Napporn, T.W. Shape-dependent electrocatalytic activity of free gold nanoparticles toward glucose oxidation. *Gold Bull.* **2013**, *46*, 311–318. [[CrossRef](#)]
60. Sribenjarat, P.; Jirakanjanakit, N.; Jirasripongpun, K. Selenium nanoparticles biosynthesized by garlic extract as antimicrobial agent. *Sci. Eng. Health Stud.* **2020**, *14*, 22–31.
61. Aljabali, A.; Akkam, Y.; Al Zoubi, M.; Al-Batayneh, K.; Al-Trad, B.; Alrob, A.O.; Alkilany, A.; Benamara, M.; Evans, D. Synthesis of gold nanoparticles using leaf extract of *Ziziphus zizyphus* and their antimicrobial activity. *Nanomaterials* **2018**, *8*, 174. [[CrossRef](#)]
62. Boruah, J.S.; Devi, C.; Hazarika, U.; Reddy, P.V.B.; Chowdhury, D.; Barthakur, M.; Kalita, P. Green synthesis of gold nanoparticles using an antiepileptic plant extract: In vitro biological and photo-catalytic activities. *RSC Adv.* **2021**, *11*, 28029–28041. [[CrossRef](#)]
63. Ameen, F.; Al-Maary, K.S.; Almansob, A.; AlNadhari, S. Antioxidant, antibacterial and anticancer efficacy of *Alternaria chlamydospora*-mediated gold nanoparticles. *Appl. Nanosci.* **2022**. [[CrossRef](#)]
64. Boomi, P.; Ganesan, R.M.; Poorani, G.; Prabu, H.G.; Ravikumar, S.; Jeyakanthan, J. Biological synergy of greener gold nanoparticles by using *Coleus aromaticus* leaf extract. *Mater. Sci. Eng. C-Mater. Biol. Appl.* **2019**, *99*, 202–210. [[CrossRef](#)]
65. Mollick, M.M.R.; Rana, D.; Dash, S.K.; Chattopadhyay, S.; Bhowmick, B.; Maity, D.; Mondal, D.; Pattanayak, S.; Roy, S.; Chakraborty, M.; et al. Studies on green synthesized silver nanoparticles using *Abelmoschus esculentus* (L.) pulp extract having anticancer (in vitro) and antimicrobial applications. *Arab. J. Chem.* **2019**, *12*, 2572–2584. [[CrossRef](#)]
66. Hassan, S.E.; Fouda, A.; Saied, E.; Farag, M.M.S.; Eid, A.M.; Barghoth, M.G.; Awad, M.A.; Hamza, M.F.; Awad, M.F. *Rhizopus oryzae*-mediated green synthesis of magnesium oxide nanoparticles (MgO-NPs): A promising tool for antimicrobial, mosquitocidal action, and tanning effluent treatment. *J. Fungi* **2021**, *7*, 372. [[CrossRef](#)] [[PubMed](#)]
67. Tomaszewska, E.; Soliwoda, K.; Kadziola, K.; Tkacz-Szczesna, B.; Celichowski, G.; Cichomski, M.; Szmaja, W.; Grobelny, J. Detection limits of DLS and UV-Vis spectroscopy in characterization of polydisperse nanoparticles colloids. *J. Nanomater.* **2013**, *2013*, 313081. [[CrossRef](#)]
68. Danaei, M.; Dehghankhold, M.; Ataei, S.; Hasanzadeh Davarani, F.; Javanmard, R.; Dokhani, A.; Khorasani, S.; Mozafari, M.R. Impact of Particle Size and Polydispersity Index on the Clinical Applications of Lipidic Nanocarrier Systems. *Pharmaceutics* **2018**, *10*, 57. [[CrossRef](#)] [[PubMed](#)]
69. Kaszuba, M.; Corbett, J.; Watson, F.M.; Jones, A. High-concentration zeta potential measurements using light-scattering techniques. *Philos. Trans. R. Soc. A-Math. Phys. Eng. Sci.* **2010**, *368*, 4439–4451. [[CrossRef](#)] [[PubMed](#)]
70. Bhattacharjee, S. DLS and zeta potential—What they are and what they are not? *J. Control. Release* **2016**, *235*, 337–351. [[CrossRef](#)]
71. Khademi-Azandehi, P.; Moghaddam, J. Green synthesis, characterization and physiological stability of gold nanoparticles from *Stachys lavandulifolia* Vahl extract. *Particuology* **2015**, *19*, 22–26. [[CrossRef](#)]
72. Nasrollahzadeh, M.; Sajadi, S.M. Green synthesis of Pd nanoparticles mediated by *Euphorbia thymifolia* L. leaf extract: Catalytic activity for cyanation of aryl iodides under ligand-free conditions. *J. Colloid Interface Sci.* **2016**, *469*, 191–195. [[CrossRef](#)]
73. Dhanjal, S.; Cameotra, S.S. Aerobic biogenesis of selenium nanospheres by *Bacillus cereus* isolated from coalmine soil. *Microb. Cell Factories* **2010**, *9*, 52. [[CrossRef](#)]
74. Kurrey, R.; Deb, M.K.; Shrivastava, K.; Khalkho, B.R.; Nirmalkar, J.; Sinha, D.; Jha, S. Citrate-capped gold nanoparticles as a sensing probe for determination of cetyltrimethylammonium surfactant using FTIR spectroscopy and colorimetry. *Anal. Bioanal. Chem.* **2019**, *411*, 6943–6957. [[CrossRef](#)]
75. Gurunathan, S.; Han, J.; Park, J.H.; Kim, J.H. A green chemistry approach for synthesizing biocompatible gold nanoparticles. *Nanoscale Res. Lett.* **2014**, *9*, 248. [[CrossRef](#)]
76. Cioran, A.M.; Teixidor, F.; Krpetić, Ž.; Brust, M.; Viñas, C. Preparation and characterization of Au nanoparticles capped with mercaptocarboranyl clusters. *Dalton Trans.* **2014**, *43*, 5054–5061. [[CrossRef](#)] [[PubMed](#)]
77. Hamza, M.F.; Hamad, D.M.; Hamad, N.A.; Abdel-Rahman, A.A.H.; Fouda, A.; Wei, Y.Z.; Guibal, E.; El-Etrawy, A.S. Functionalization of magnetic chitosan microparticles for high-performance removal of chromate from aqueous solutions and tannery effluent. *Chem. Eng. J.* **2022**, *428*, 131775. [[CrossRef](#)]
78. Zaaeri, F.; Khoobi, M.; Rouini, M.; Javar, H.A. pH-responsive polymer in a core-shell magnetic structure as an efficient carrier for delivery of doxorubicin to tumor cells. *Int. J. Polym. Mater. Polym. Biomater.* **2018**, *67*, 967–977. [[CrossRef](#)]
79. Jin, W.; Shen, D.K.; Liu, Q.; Xiao, R. Evaluation of the co-pyrolysis of lignin with plastic polymers by TG-FTIR and Py-GC/MS. *Polym. Degrad. Stab.* **2016**, *133*, 65–74. [[CrossRef](#)]
80. Sakugawa, K.; Ikeda, A.; Takemura, A.; Ono, H. Simplified method for estimation of composition of alginates by FTIR. *J. Appl. Polym. Sci.* **2004**, *93*, 1372–1377. [[CrossRef](#)]
81. Lawrie, G.; Keen, I.; Drew, B.; Chandler-Temple, A.; Rintoul, L.; Fredericks, P.; Grondahl, L. Interactions between alginate and chitosan biopolymers characterized using FTIR and XPS. *Biomacromolecules* **2007**, *8*, 2533–2541. [[CrossRef](#)] [[PubMed](#)]
82. Dang, Y.R.; Bediako, J.K.; Lin, X.Y.; Choi, J.W.; Lim, C.R.; Song, M.H.; Han, M.; Yun, Y.S. Polyethyleneimine impregnated alginate capsule as a high capacity sorbent for the recovery of monovalent and trivalent gold. *Sci. Rep.* **2021**, *11*, 17836. [[CrossRef](#)] [[PubMed](#)]

83. Saxena, N.; Pal, N.; Ojha, K.; Dey, S.; Mandal, A. Synthesis, characterization, physical and thermodynamic properties of a novel anionic surfactant derived from *Sapindus laurifolius*. *RSC Adv.* **2018**, *8*, 24485–24499. [[CrossRef](#)]
84. Hamza, M.F.; Salih, K.A.M.; Abdel-Rahman, A.A.H.; Zayed, Y.E.; Wei, Y.Z.; Liang, J.; Guibal, E. Sulfonic-functionalized algal/PEI beads for scandium, cerium and holmium sorption from aqueous solutions (synthetic and industrial samples). *Chem. Eng. J.* **2021**, *403*, 126399. [[CrossRef](#)]
85. Wani, I.A.; Ahmad, T. Size and shape dependant antifungal activity of gold nanoparticles: A case study of *Candida*. *Colloids Surf. B-Biointerfaces* **2013**, *101*, 162–170. [[CrossRef](#)]
86. Folorunso, A.; Akintelu, S.; Oyebamiji, A.K.; Ajayi, S.; Abiola, B.; Abdusalam, I.; Morakinyo, A. Biosynthesis, characterization and antimicrobial activity of gold nanoparticles from leaf extracts of *Annona muricata*. *J. Nanostructure Chem.* **2019**, *9*, 111–117. [[CrossRef](#)]
87. Senthilkumar, S.; Kashinath, L.; Ashok, M.; Rajendran, A. Antibacterial properties and mechanism of gold nanoparticles obtained from *Pergularia aemia* leaf extract. *J. Nanomed. Res.* **2017**, *6*, 146. [[CrossRef](#)]
88. Job, V.; Laloy, J.; Maloteau, V.; Haye, E.; Lucas, S.; Penninckx, S. Investigation of the Antibacterial Properties of Silver-Doped Amorphous Carbon Coatings Produced by Low Pressure Magnetron Assisted Acetylene Discharges. *Int. J. Mol. Sci.* **2022**, *23*, 563. [[CrossRef](#)] [[PubMed](#)]
89. Mussin, J.; Robles-Botero, V.; Casañas-Pimentel, R.; Rojas, F.; Angiolella, L.; San Martín-Martínez, E.; Giusiano, G. Antimicrobial and cytotoxic activity of green synthesis silver nanoparticles targeting skin and soft tissue infectious agents. *Sci. Rep.* **2021**, *11*, 14566. [[CrossRef](#)] [[PubMed](#)]
90. Kowalska-Krochmal, B.; Dudek-Wicher, R. The minimum inhibitory concentration of antibiotics: Methods, interpretation, clinical relevance. *Pathogens* **2021**, *10*, 165. [[CrossRef](#)] [[PubMed](#)]
91. Fouda, A.; Awad, M.A.; Eid, A.M.; Saied, E.; Barghoth, M.G.; Hamza, M.F.; Awad, M.F.; Abdelbary, S.; Hassan, S.E. An eco-friendly approach to the control of pathogenic microbes and *Anopheles stephensi* malarial vector using magnesium oxide nanoparticles (Mg-NPs) fabricated by *Penicillium chrysogenum*. *Int. J. Mol. Sci.* **2021**, *22*, 5096. [[CrossRef](#)] [[PubMed](#)]
92. Slavin, Y.N.; Asnis, J.; Hafeli, U.O.; Bach, H. Metal nanoparticles: Understanding the mechanisms behind antibacterial activity. *J. Nanobiotechnol.* **2017**, *15*, 65. [[CrossRef](#)]
93. Wang, L.L.; Hu, C.; Shao, L.Q. The antimicrobial activity of nanoparticles: Present situation and prospects for the future. *Int. J. Nanomed.* **2017**, *12*, 1227–1249. [[CrossRef](#)]
94. Li, Y.; Zhang, W.; Niu, J.F.; Chen, Y.S. Mechanism of photogenerated reactive oxygen species and correlation with the antibacterial properties of engineered metal-oxide nanoparticles. *ACS Nano* **2012**, *6*, 5164–5173. [[CrossRef](#)]
95. Lv, Q.Z.; Yan, L.; Jiang, Y.Y. The synthesis, regulation, and functions of sterols in *Candida albicans*: Well-known but still lots to learn. *Virulence* **2016**, *7*, 649–659. [[CrossRef](#)]
96. Mohamed, A.E.; Elgammal, W.E.; Eid, A.M.; Dawaba, A.M.; Ibrahim, A.G.; Fouda, A.; Hassan, S.M. Synthesis and characterization of new functionalized chitosan and its antimicrobial and in-vitro release behavior from topical gel. *Int. J. Biol. Macromol.* **2022**, *207*, 242–253. [[CrossRef](#)] [[PubMed](#)]
97. Oueslati, M.H.; Ben Tahar, L.; Harrath, A.H. Catalytic, antioxidant and anticancer activities of gold nanoparticles synthesized by kaempferol glucoside from *Lotus leguminosae*. *Arab. J. Chem.* **2020**, *13*, 3112–3122. [[CrossRef](#)]
98. Boomi, P.; Ganesan, R.; Poorani, G.P.; Jegatheeswaran, S.; Balakumar, C.; Prabu, H.G.; Anand, K.; Prabhu, N.M.; Jeyakanthan, J.; Saravanan, M. Phyto-engineered gold nanoparticles (AuNPs) with potential antibacterial, antioxidant, and wound healing activities under in vitro and in vivo conditions. *Int. J. Nanomed.* **2020**, *15*, 7553–7568. [[CrossRef](#)] [[PubMed](#)]
99. Markus, J.; Wang, D.; Kim, Y.-J.; Ahn, S.; Mathiyalagan, R.; Wang, C.; Yang, D.C. Biosynthesis, characterization, and bioactivities evaluation of silver and gold nanoparticles mediated by the roots of chinese herbal *Angelica pubescens* Maxim. *Nanoscale Res. Lett.* **2017**, *12*, 46. [[CrossRef](#)] [[PubMed](#)]
100. Penninckx, S.; Heuskin, A.-C.; Michiels, C.; Lucas, S. Gold Nanoparticles as a Potent Radiosensitizer: A Transdisciplinary Approach from Physics to Patient. *Cancers* **2020**, *12*, 2021. [[CrossRef](#)] [[PubMed](#)]
101. Vardakas, P.; Kyriazis, I.D.; Kourti, M.; Skaperda, Z.; Tekos, F.; Kouretas, D. Chapter 6—Oxidative stress-mediated nanotoxicity: Mechanisms, adverse effects, and oxidative potential of engineered nanomaterials. In *Advanced Nanomaterials and Their Applications in Renewable Energy*, 2nd ed.; Liu, J.L., Yan, T.-H., Bashir, S., Eds.; Elsevier: Amsterdam, The Netherlands, 2022; pp. 179–218. [[CrossRef](#)]
102. Kim, S.; Ryu, D.Y. Silver nanoparticle-induced oxidative stress, genotoxicity and apoptosis in cultured cells and animal tissues. *J. Appl. Toxicol. JAT* **2013**, *33*, 78–89. [[CrossRef](#)]
103. Manke, A.; Wang, L.; Rojanasakul, Y. Mechanisms of nanoparticle-induced oxidative stress and toxicity. *Biomed Res. Int.* **2013**, *2013*, 942916. [[CrossRef](#)]
104. Eid, A.M.; Fouda, A.; Niedbala, G.; Hassan, S.E.-D.; Salem, S.S.; Abdo, A.M.; Hetta, H.F.; Shaheen, T.I. Endophytic *Streptomyces laurentii* mediated green synthesis of Ag-NPs with antibacterial and anticancer properties for developing functional textile fabric properties. *Antibiotics* **2020**, *9*, 641. [[CrossRef](#)]
105. Steckiewicz, K.P.; Barcinska, E.; Malankowska, A.; Zauszkiewicz-Pawlak, A.; Nowaczyk, G.; Zaleska-Medynska, A.; Inkielewicz-Stepniak, I. Impact of gold nanoparticles shape on their cytotoxicity against human osteoblast and osteosarcoma in in vitro model. Evaluation of the safety of use and anti-cancer potential. *J. Mater. Sci. -Mater. Med.* **2019**, *30*, 22. [[CrossRef](#)]

106. Surapaneni, S.K.; Bashir, S.; Tikoo, K. Gold nanoparticles-induced cytotoxicity in triple negative breast cancer involves different epigenetic alterations depending upon the surface charge. *Sci. Rep.* **2018**, *8*, 12295. [[CrossRef](#)]
107. Marzouni, H.Z.; Davachi, B.; Rezazadeh, M.; Milani, M.S.; Matinfard, S. Diagnostic value of hepatic vein ultrasound in early detection of liver cirrhosis. *Galen Med. J.* **2018**, *7*, e1140. [[CrossRef](#)]
108. Chang, Y.; Zheng, C.; Chinnathambi, A.; Alahmadi, T.A.; Alharbi, S.A. Cytotoxicity, anti-acute leukemia, and antioxidant properties of gold nanoparticles green-synthesized using *Cannabis sativa* L. leaf aqueous extract. *Arab. J. Chem.* **2021**, *14*, 103060. [[CrossRef](#)]
109. El-Borady, O.M.; Ayat, M.S.; Shabrawy, M.A.; Millet, P. Green synthesis of gold nanoparticles using Parsley leaves extract and their applications as an alternative catalytic, antioxidant, anticancer, and antibacterial agents. *Adv. Powder Technol.* **2020**, *31*, 4390–4400. [[CrossRef](#)]
110. Jeyarani, S.; Vinita, N.M.; Puja, P.; Senthamilselvi, S.; Devan, U.; Velangani, A.J.; Biruntha, M.; Pugazhendhi, A.; Kumar, P. Biomimetic gold nanoparticles for its cytotoxicity and biocompatibility evidenced by fluorescence-based assays in cancer (MDA-MB-231) and non-cancerous (HEK-293) cells. *J. Photochem. Photobiol. B-Biol.* **2020**, *202*, 111715. [[CrossRef](#)]
111. Fouda, A.; Eid, A.M.; Abdel-Rahman, M.A.; El-Belely, E.F.; Awad, M.A.; Hassan, S.E.-D.; Al-Faifi, Z.E.; Hamza, M.F. Enhanced antimicrobial, cytotoxicity, larvicidal, and repellence activities of brown algae, *Cystoseira crinita*-mediated green synthesis of magnesium oxide nanoparticles. *Front. Bioeng. Biotechnol.* **2022**, *10*, 849921. [[CrossRef](#)] [[PubMed](#)]
112. Verma, S.K.; Nisha, K.; Panda, P.K.; Patel, P.; Kumari, P.; Mallick, M.A.; Sarkar, B.; Das, B. Green synthesized MgO nanoparticles infer biocompatibility by reducing in vivo molecular nanotoxicity in embryonic zebrafish through arginine interaction elicited apoptosis. *Sci. Total Environ.* **2020**, *713*, 136521. [[CrossRef](#)]